DIPLOMARBEIT

Titel der Diplomarbeit

„Development of an
Open CO_2 Cooling System for Belle II“

Verfasserin ODER Verfasser

Annekathrin Frankenberger

angestrebter akademischer Grad

Magistra der Naturwissenschaften (Mag. rer. nat.)

Wien, 2013

Studienkennzahl lt. Studienblatt:	A 411
Studienrichtung lt. Studienblatt:	Diplomstudium Physik
Betreuerin / Betreuer:	Univ. Prof. DI Dr. Christian Fabjan

Abstract

At the KEK (Tsukuba, Japan) a major upgrade of the accelerator system is under construction and requires a redesign of the entire Belle detector, especially of the Silicon Vertex Detector (SVD). As a consequence of the new Belle II SVD design, a new cooling concept for the sensor readout electronics is required. For thermal management of the Belle II SVD a two-phase evaporative CO_2 cooling system is under development.

In order to gain experience concerning the Belle II SVD cooling system, a less extensive and less complicated cooling plant has been developed. The key issue of this thesis is the design and construction of an open CO_2 cooling system for research, development and testing. This independent, scalable and transportable cooling plant is necessary to get familiar with CO_2 and to acquire test results which can be applied to the Belle II SVD cooling system.
One big topic is the component dimensioning and selection with the big challenge of using off-the-shelf components. Furthermore, a detailed description and explanation of the design and the assembly is given. After realizing and commissioning, the system successfully operated in various applications. Despite prevailing rough conditions in a particle detector, a well functioning but still simple design was worked out.
Other major topics of this thesis are the development of a reliable tube fixture mechanism and the investigation of a material to ensure adequate heat transfer between pipe and readout electronics. Finally, the developed cooling plant was used to verify the cooling concept by testing various sensor module prototypes in beam tests.

Kurzfassung

Am KEK (Tsukuba, Japan) wird derzeit ein Upgrade des Beschleunigersystems durchgeführt und verlangt ein Redesign des Belle Detektors, insbesondere des Silicon Vertex Detektors (SVD). Das neue Belle II SVD Design erfordert ein neues Kühlkonzept für die Ausleseelektronik der Sensoren, wofür ein zwei Phasen Verdampfungssystem auf CO_2 Basis in Entwicklung ist.

Um Erfahrungen für das Belle II SVD Kühlsystem zu sammeln, wurde ein kompaktes und vereinfachtes Kühlsystem entwickelt. Der Schwerpunkt dieser Arbeit ist das Design und die Konstruktion eines offenen CO_2 Kühlsystems für Forschungs-, Entwicklungs- und Testzwecke. Diese eigenständige, skalierbare und transportable Anlage ist notwendig, um den Umgang mit CO_2 als Kältemittel zu erlernen und Erfahrungen und Testergebnisse zu sammeln, die auf die zukünftige Belle II SVD Kühlung angewandt werden können.
Diese Arbeit beschreibt detailliert das Design und die Realisierung der Anlage, wobei Dimensionierung und Komponentenauswahl einen wesentlichen Aspekt darstellen. Hierbei wurde auf die Verwendung von Standardkomponenten Wert gelegt. Nach der Realisierung und der Inbetriebnahme des Systems wurde es in diversen Versuchsaufbauten erfolgreich eingesetzt und betrieben.Trotz der anspruchsvollen Anforderungen eines Teilchenbeschleunigers konnte ein gut funktionierendes und dennoch verhältnismäßig einfaches Design ausgearbeitet werden.
Weitere Themen dieser Arbeit sind die Entwicklung zuverlässiger Mechanismen zur Befestigung der Kühlrohre und Untersuchungen des thermischen Übergangs zwischen Ausleseelektronik und Kühlrohr. Das erarbeitete Kühlkonzept wurde abschließend mit Hilfe der entwickelten Kühlanlage an verschiedenen Sensormodulprototypen bei Beamtests evaluiert.

Contents

Chapter 1

Introduction

The High Energy Accelerator Research Organization (KEK) in Tsukuba, Japan, operated an asymmetric electron-positron collider (KEKB) [1] between 1999 and 2010. It produced B and Anti-B mesons for various studies to gain information especially about the CP violation in the B-meson decay. The CP violation [2] was proposed by Makoto Kobayashi and Toshihide Maskawa, both received the physics Nobel Prize in 2008 for this work. The KEKB accelerator and the Belle collaboration made significant contributions to validate this proposal.
Following this great success, an upgrade of the KEKB accelerator and the Belle detector [3] was planned with the aim to reach 40 times higher luminosity compared to the previous system with an ultimate target of $8 \times 10^{35}\text{cm}^{-2}\text{s}^{-1}$. This upgrade is required in order to allow precise studies of rare decays, gaining insight to new physics beyond the standard model. Consequently, the Belle experiment has to be improved which implies a completely new Silicon Vertex Detector (SVD[1]), together with the Pixel Detector (PXD) the innermost subdetector of the Belle experiment. The upgrade leads to the new SuperKEKB [4] accelerator and the Belle II detector [5].

The Viennese Institute of High Energy Physics (HEPHY), which belongs to the Austrian Academy of Sciences, is a member of the international Belle collaboration, working on this project. HEPHY has global responsibility for the SVD design and construction. Compared to the previous Silicon Vertex Detector, one major achievement of the new SVD is the newly developed Origami chip-on-sensor design and an extremely light ladder support structure. This design requires a new cooling concept for which a two-phase evaporative CO_2 cooling was found to be the most suitable.

This work deals with the development of an open CO_2 cooling system, including a conceptual design, the component dimensioning and selection and the final assembly. This development is mandatory to gain experience and test results which can be applied to the SVD cooling and detector design.
The content of this thesis is arranged as follows. Chapter two refers to the KEKB accelerator system and describes the KEKB collider, the former Belle and the upgraded

[1] The new Belle II Silicon Vertex Detector conveniently is called SVD.

Belle II detectors. It also provides detailed information about the SVD mechanical structure. Chapter three presents information about the SVD cooling. Subsequently, the open CO_2 cooling system is addressed in chapter four. All cooling requirements, the functional principle, component selection and test results are presented in detail. Chapter five handles various tube mounting and heat conductive material issues regarding the Origami cooling design and presents several solutions. The last chapter summarizes the achievements and problems of the open CO_2 cooling system design and construction.

Chapter 2

The KEKB Accelerator System

The KEKB accelerator system consists of the KEKB accelerator and the Belle detector comprising several subdetectors. It is located at the KEK research laboratory in Tsukuba, Japan which was established in 1971. After the operation of several other accelerators and experiments, the KEKB accelerator became operational in 1998 and the Belle experiment started in 1999.

2.1 The KEKB Particle Accelerator

The B-factory KEKB [1] is an asymmetric electron-positron collider, producing B and Anti-B mesons. The two synchrotron rings storing the beams have a circumference of 3km. The high energy ring (HER) for the electrons at 8GeV and the low energy ring (LER) for the positrons at 3.5GeV are installed side by side in a tunnel and cross each other at the interaction point (IP). The Belle detector at the Tsukuba experimental hall surrounds the IP, registering the particles arising from the e^+ - e^- collisions. After the commissioning in the end of 1998, data were collected from June 1999 until the shutdown in June 2010. The performance of the accelerator was steadily improved, resulting in a peak luminosity of $2.1 \times 10^{34}\text{cm}^{-2}\text{s}^{-1}$, which is twice the design value.

High luminosity is a major aspect to gain excellent research results by statistics. The luminosity of a collider is a measure of its efficiency and depends on the accelerator structure and the particle beam quality. The higher the luminosity, the more particles are available for collisions. The luminosity is defined as the number of events in the detector per cross section with the unit $cm^{-2}s^{-1}$.
The Luminosity $\mathcal{L}$ of a collider is calculated as described by equation 2.1 [5], assuming flat beams and equal beam sizes in horizontal and vertical directions:

$$\mathcal{L} = \frac{\gamma_\pm}{2er_e}\left(\frac{I_\pm \xi_{y\pm}}{\beta^*_{y\pm}}\right)\left(\frac{R_L}{R_{\xi_y}}\right) \tag{2.1}$$

In equation 2.1 $\gamma_\pm$ are the Lorentz factors of the electron and positron beams, e is the elementary electric charge and r_e the classical electron radius. $I_\pm$ are the currents of the electron and positron beams. $\xi_{y\pm}$ are the vertical beam-beam parameters, R_L and R_y are luminosity and vertical beam parameter reduction factors, which refer to the crossing angle and the hourglass effect. β_y^* is the vertical beta function at the IP. The main determining parameters for the luminosity are the total beam current, the vertical beam parameter and the vertical beta function at the IP.

The collaboration is currently working on a major upgrade of the KEKB accelerator, the SuperKEKB (figure 2.1), to achieve higher luminosity. This increased luminosity results from the nano-beam design based on the idea of P. Ramondi, Frascati [6] with a smaller beam size at the IP by lowering β and increasing the currents $I_\pm$. Compared to the previous KEKB, the vertical beta functions are reduced by almost a factor of 20 and the beam currents are doubled. This upgrade was first announced in 2003 and the groundbreaking ceremony took place in 2011. In this improved implementation, the electron-positron beams collide at 7GeV and 4GeV with the design luminosity of $8 \times 10^{35}\text{cm}^{-2}\text{s}^{-1}$.

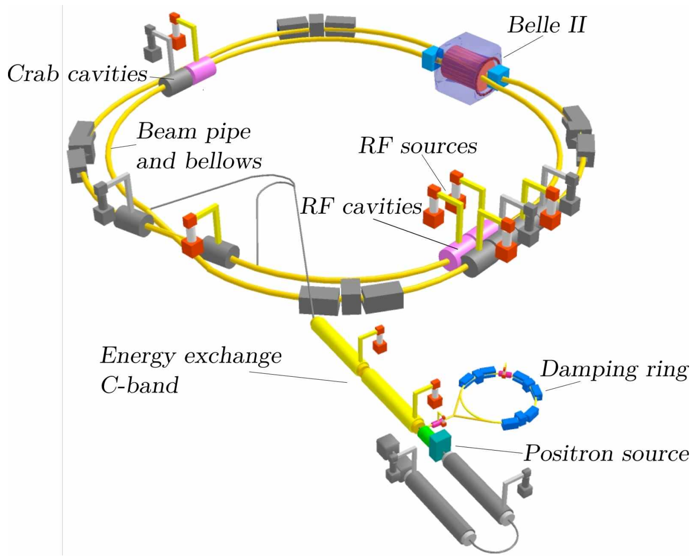

Figure 2.1: Schematic view of the SuperKEKB accelerator system. [7] modified

2.2 The Belle/Belle II Detector

The achievement of higher luminosity implies an increased occupancy of the detector channels and radiation dose. To cope with that, an upgrade of the former Belle detector was considered and first ideas were presented in 2004 [7]. Measurements with higher sensitivity and an improved precision will be possible with the new Belle II experiment which consists of several subdetectors. Figure 2.2 depicts the new Belle II detector, with new or refurbished subdetectors.

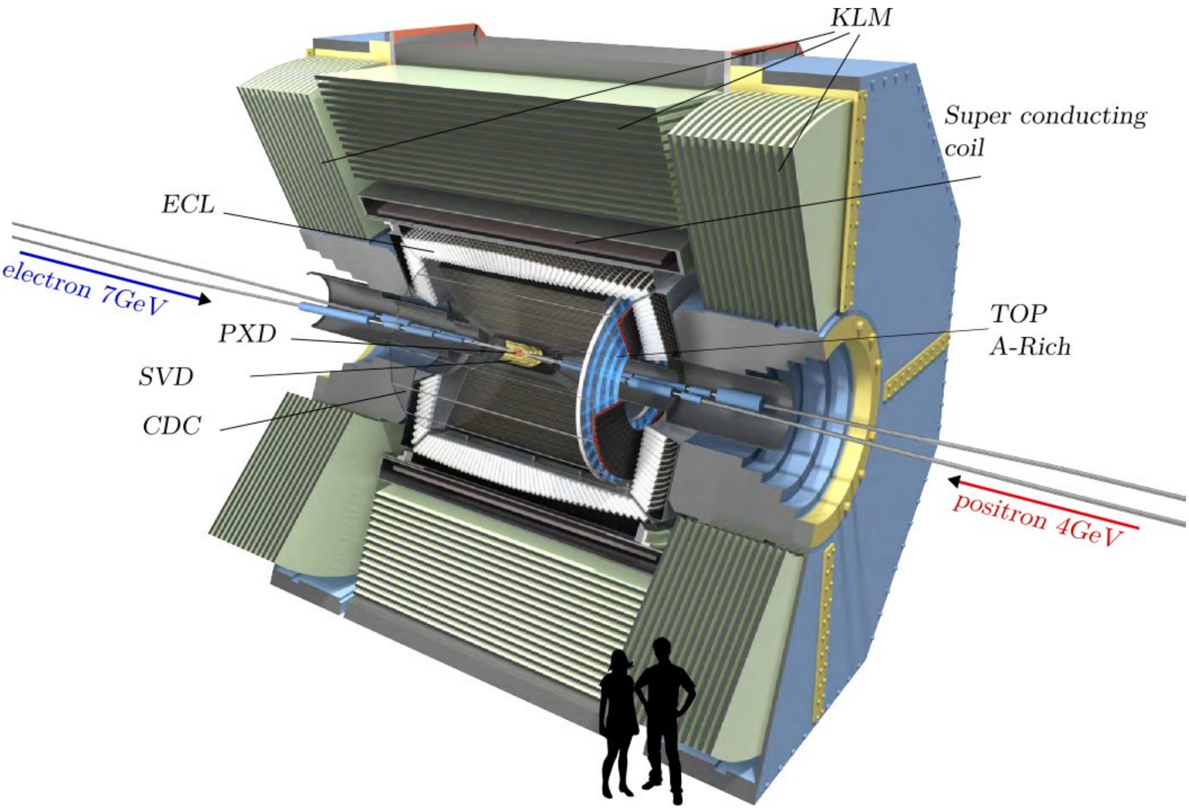

Figure 2.2: Structure of the Belle II detector.
[8]

The PXD and the SVD are the innermost subdetectors. These vertex detectors are responsible for the decay vertex measurement of the B-mesons as well as D and τ particles. The SVD is surrounded by a central drift chamber (CDC) to track charged particles by measuring their trajectories, momenta and provides also dE/dx information. Besides that, the surrounding Aerogel Cherenkov counters (A-RICH) at the forward side and the Time of Propagation counters (TOP) in the barrel detector part are responsible for the charged particle identification. For the detection of electromagnetic showers, CsI(Tl) scintillator crystals remain inside the superconducting solenoid coil in the barrel part and pure CsI crystals are added in the endcap. An array of resistive plate chambers, attached to the outer iron yoke, identifies muons and K_L mesons.

The Belle II detector features a new vertexing concept with a pixel detector [9] based on DEPFET (DEPleted Field Effect Transistor) technology in addition to the SVD. In order to place two new PXD layers directly surrounding the beam pipe, the new SVD is designed with increased radii. Its development has started by the end of 2008 and it is scheduled to become operational until 2015.

2.3 Semiconductor Detectors

Semiconductor detectors are widely-used in High Energy and Nuclear Physics for energy measurements, gamma spectroscopy, vertexing and tracking. Semiconductor detectors feature precise measuring because of their excellent spatial resolution and fast signaling. Moreover, they profit from the highly sophisticated semiconductor industry.

The detection of ionizing radiation with semiconductors can be described as follows. Electrons from the valence band are stimulated by an ionizing particle and lifted from the valence band into the conduction band. This creates free electron-hole pairs in the semiconductor material, resulting in a measurable current if an electrical field is applied. The conductivity of semiconductors highly depends on the operating temperature. A pure semiconductor is an insulator at absolute zero and it gets conductive as the temperature increases. At temperatures above absolute zero, electrons from the valence band get thermally excited and can reach the conduction band. The intensity of this effect depends on the band gap of the semiconductor material. In the case of silicon, the band gap at room temperature is 1.12eV. The average energy to create an electron-hole pair as a function of the band gap energy can be seen in figure 2.3.

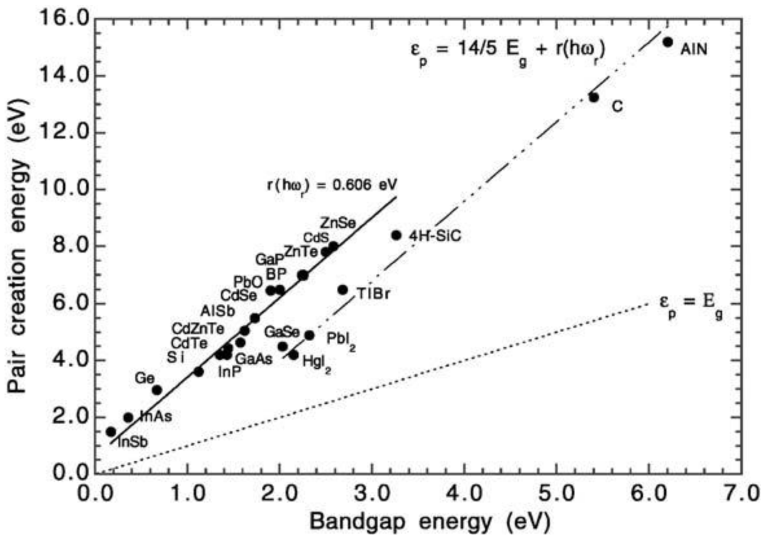

Figure 2.3: Average energy to create an electron-hole pair as a function of the band gap energy for various semiconductors and further aluminum nitride (AlN) and diamond (C).

[10]

To prevent leakage currents due to thermal excitation, semiconductor detectors must be doped and reverse biased. Joining p and n doped zones results in a diode structure and a depletion zone which is free of charge carriers when reverse biased. By applying a dedicated reverse voltage the potential difference between the p/n junction prevents leakage currents due to thermal excitation. On that account, reverse biased diodes, deployed as particle detectors, only measure currents if electron-hole pairs are created

by external stimulus, e.g. a particle hitting the detector.
In High Energy Physics, two different architectures of semiconductor detectors are very common. Both, the strip and the pixel designs enable precise particle tracking. Figure 2.4 shows the electrode segmentation of a silicon strip sensor. In addition to this one-dimensional strip segmentation, pixel detectors feature a two-dimensional checkered pattern segmentation. To collect the generated charges, every strip/pixel must be connected to the readout electronics. The strip size as well as the pixel size is a meaningful parameter for the spatial detector resolution with typical values in the rage of several tens to hundreds of μm, e.g. 75μm and 240μm for the majority of the SVD strip sensors.

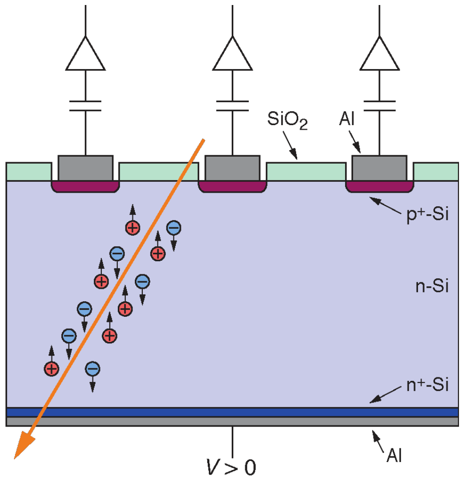

Figure 2.4: Schematic view of a silicon strip detector with a traversing ionizing particle. [11]

A schematic view of a silicon strip detector is depicted in figure 2.4 with low n-doped silicon bulk material and electrodes, consisting of highly doped n^+ and p^+ bulks. An aluminum metallization is applied for an electrical connection of each individual detector strip to the readout electronics. The n^+-layer on the bottom side of the detector provides an Ohmic contact. An ionizing particle, illustrated by the orange arrow, creates electron-hole pairs in the depleted Si substrate while passing the detector. Under the influence of the electric field, the electrons drift towards the n^+ layer and the holes towards the p^+ layer, inducing a signal while they move. The different signals induced in discrete strips provide information about the particle position.
An advanced common sensor architecture, which is used in the SVD, is the double-sided strip detector (DSSD) arrangement. It is a two dimensional sensor, on which the strips are arranged orthogonally on both detector sides. A schematic view of such a DSSD is shown in figure 2.5.

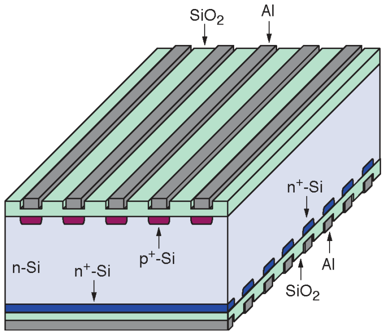

Figure 2.5: Schematic view of a double-sided silicon strip detector. (The illustration does not show biasing structures) [11]

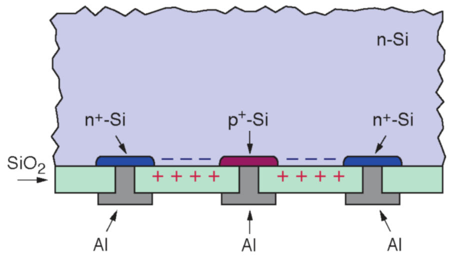

Figure 2.6: Schematic view of a p stop implant at the n side of a silicon detector. ([11] modified)

Figure 2.5 shows that the p^+ doped electrodes are isolated automatically against each other by the n-substrate. In case of the n^+ strips on the bottom side, an additional isolation between the n^+ electrodes is required to avoid shorts. So called p stop structures available in different layouts [12] are used for an insulation of the n^+ doped strips towards each other (figure 2.6).
A major issue of DSSDs is the appearance of ambiguous data with simultaneously[1] traversing particles. Figure 2.7 depicts one example of such ghost hits with two simultaneously traversing particles P_1 and P_2. They induce signals at the strips p^+-2, p^+-4, n^+-2 and n^+-3, representing four possible traversing positions, where two points are ghost hits which have to be eliminated. Despite these ghost hits, the track reconstruction of the real particle can be determined with data from several other detector layers.

[1]In this context, simultaneously refers to the integration time of the readout electronics.

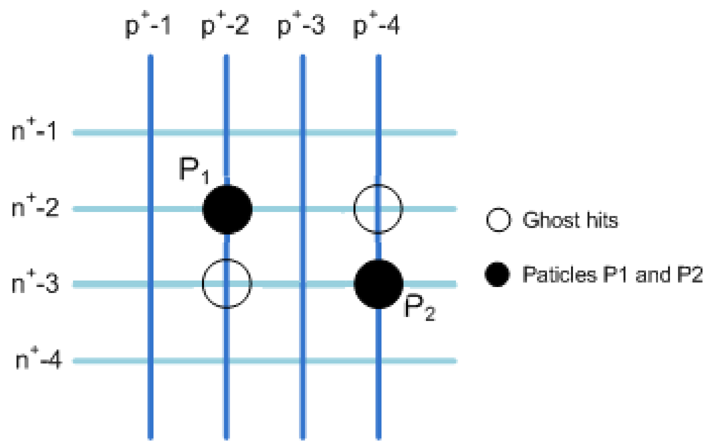

Figure 2.7: The four possible positions of two simultaneously traversing particles (circles P_1 and P_2), traversing a double-sided strip sensor. n^+ and p^+, the different implanted strips orthogonally opposed on the two sides, are marked with the light and dark blue lines.

This detector architecture is a compromise between unambiguous measurements, costs and complexity. Compared to strip detectors, pixel detectors provide unambiguous two-dimensional measurements but therefore need a more complex sensor design together with an extremely high number of readout channels.

The silicon detector size is limited by the semiconductor wafer processing capability, which is presently limited to 6". To get an accurate picture of the particle tracks in collision experiments, multiple strip detectors must be arranged together.

2.4 Belle II Silicon Vertex Detector

The SVD is required to be low-mass, highly precise, immune to background hits, radiation tolerant, mechanically stable, efficiently cooled and reliable operating over its lifetime of at least ten years. The mechanical details of the SVD are given by I. Gfall [13]. The SVD has an outer diameter of 270mm and surrounds the PXD. Like its predecessor, it is equipped with DSSDs but with increased sensor size. The Belle II polar angular acceptance region is $17° < \vartheta < 150°$. The previous cylindrical design was replaced by an asymmetrically lantern shaped geometry, keeping the sensor and channel count and the material as low as possible.
Figure 2.8 depicts the CAD design of the SVD where adjacent ladders are overlapping, forming a windmill detector structure, to allow a precise ladder alignment. The SuperKEKB is a relatively low energy machine, where the particles arising from collisions are prone to multiple scattering. This results in distorted particle tracks which are unsuitable for the alignment procedure and therefore high energetic cosmic muons are used for this purpose. To allow a convenient alignment with rare cosmic muons, a sufficient overlap must be balanced against the material budget.

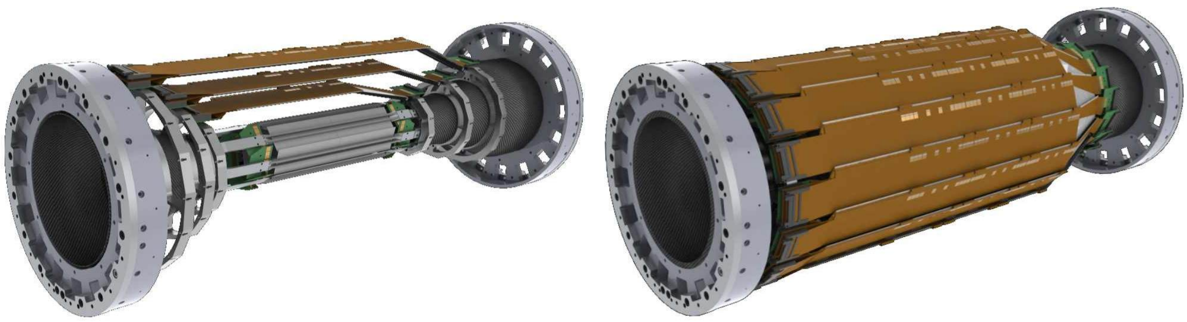

Figure 2.8: CAD design of the four SVD layers.

All ladders are mounted on two separable end rings. The new SVD lantern shape is divided into the slanted part (the forward side) of the detector and the barrel part. The SVD consists of four layers as illustrated in figure 2.9, where also the PXD is marked (blue). The SVD numbering starts with the innermost layer three, up to the outermost layer six.

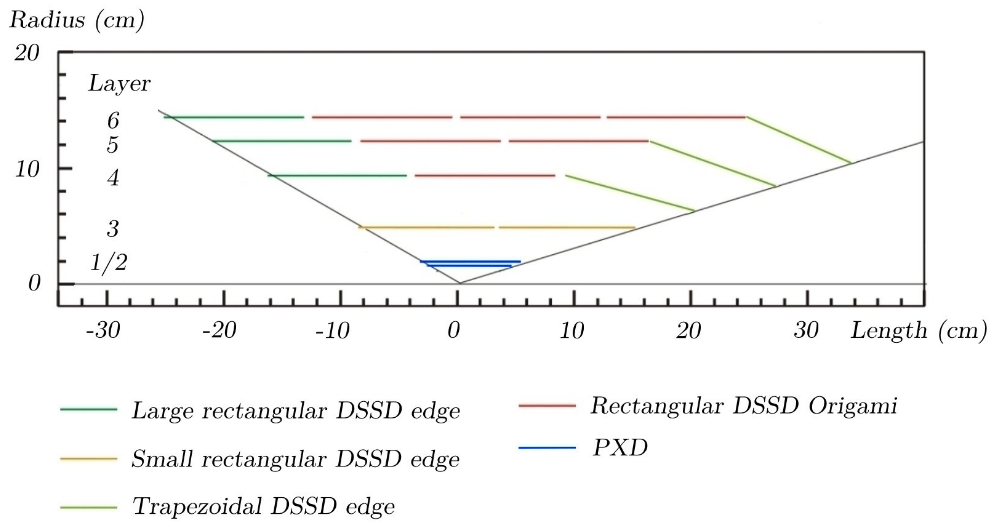

Figure 2.9: Configuration of four SVD and two PXD layers. ([5] modified)

Each ladder consists of a varying number of DSSDs with different shapes. Trapezoidal shaped sensors (light green) in layers four, five and six cover the forward detector region. Rectangular sensors are installed in layer three (orange) and the barrel parts of layers four, five and six (dark green and red).
Another differentiation which must be made is the placement of the readout electronics. At the edge DSSDs (orange, light green, dark green), readout chips (RO chips) are assembled outside the acceptance region, whereas the RO chips of the inner rectangular DSSDs (red) are directly assembled on top of the sensor modules. Figures 2.10, 2.11 and 2.12 depict the structure of a layer six ladder, an assembled Origami module and hybrid boards.

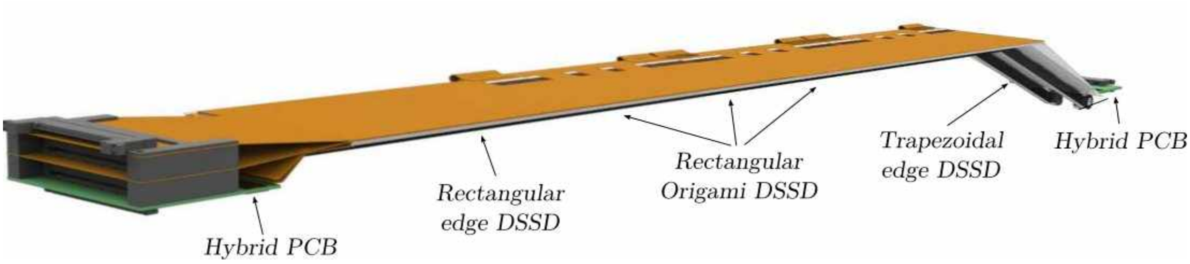

Figure 2.10: SVD layer six ladder.

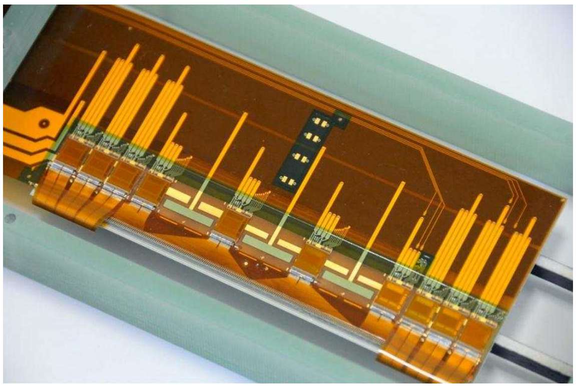

Figure 2.11: An assembled Origami DSSD module.

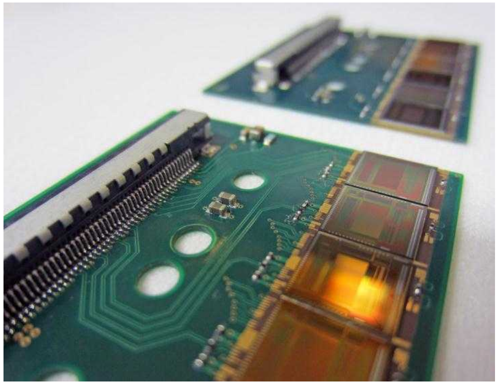

Figure 2.12: Hybrid boards for the edge sensors.

The DSSDs of the respective ladders are assembled on two lightweight composite sandwich carbon fiber ribs. Table 2.1 gives the radii of the different layers and the number of ladders, DSSDs and RO chips of the SVD.

Layer	**Radius (mm)**	**Ladder**	**DSSDs/ ladder**	**DSSDs**	**RO chips/ DDSD**	**RO chips total**
6	135	16	5	80	10	800
5	104	12	4	48	10	480
4	80	10	3	30	10	300
3	38	7	2	14	12	168
Sum		**45**		**172**		**1748**

Table 2.1: The SVD layout with assembly details.
[13]

After describing the general mechanical structure of the SVD, the upcoming section deals with some details of the DSSD structure. The Belle II DSSDs are made from n-type doped silicon, manufactured in a p-on-n process with p-stop blocking technique for an electrical separation of the n doped electrodes on the n side (section 2.3). The strip arrangement of an Origami DSSD can be seen in figure 2.13. The long strips are on the p side, facing the beam pipe. The p strips, arranged in parallel to the beam axis (z-axis), measure the $r - \phi$ coordinate of the traversing particle and the n strips (on the opposite side) determine the z coordinate.

For the signal processing, special readout chips are necessary because of the very low signal levels. Each sensor strip is connected to a separate input channel of the RO chip by wire bonding with an ultrasonic welding method. An absolutely essential feature of the SVD RO chips is a fast shaping time, suppressing off-time background hits. Thus, the APV25 [14] chip, which was developed and deployed for the CMS (Compact Muon Solenoid) Silicon Tracker, has been chosen for the SVD. In the following this APV25 RO chips conveniently are called APVs.
The desired fast shaping time, together with noise considerations requires a chip-on-sensor design for the inner sensors, leading to a minimized input capacitance. This new, so called Origami chip-on-sensor design (figures 2.11 and 2.13) entails more material in the acceptance region compared to the former SVD but is the only solution to achieve the required signal-to-noise ratio combined with a fast shaping time and thus low occupancy. Contrary to that, edge sensors use conventional PCB hybrids (figure 2.12) outside the acceptance region, on which the RO chips are assembled and connected to the edge sensor strips.

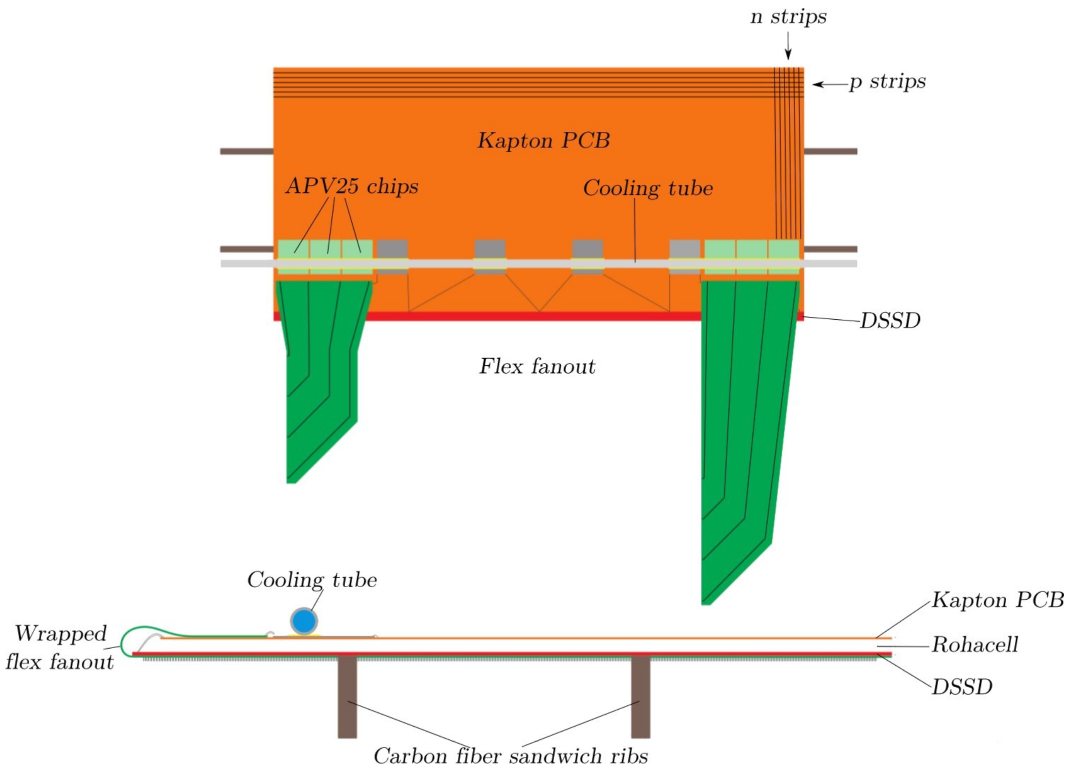

Figure 2.13: Top and side view of the Origami chip-on-sensor concept. ([5] modified)

All Origami APVs are arranged in a single row along the sensor and glued on top of the Kapton PCB (figure 2.13). There, the top side n strips are connected by pitch adapters to the APVs. The p strips from the bottom sensor side are connected by flexible Kapton fan-outs wrapped around the edge of the sensors.
The heat generation caused by the APVs would lead to a heat accumulation if no active cooling is installed. Therefore a cooling pipe must be routed through the active detector volume. A low APV temperature of the RO electronics is essential for a reasonable data taking with a high signal to noise ratio. The cooling requirements and concepts for the SVD cooling are described in the following chapter 3, which gives an overview of the determining factors concerning the development of the open CO_2 cooling system.

Chapter 3

Belle II SVD Cooling

The cooling of electronic components is crucial in many applications. In case of the Belle II detector very sophisticated semiconductor electronics are used and require active cooling. The two subdetectors SVD and PXD have a common coolant supply, but can be considered as individual sub systems. This thesis covers only the SVD therefore the PXD cooling will not be further mentioned.
This chapter introduces and analyzes the general SVD cooling concept as well as the requirements, which are needed in order to deduce the special requirements for the open CO_2 cooling system. In addition, the most important questions which arise regarding the general approach of this development will be answered and a general understanding for the underlying conditions will be given.

3.1 Sensor Module Cooling Concept

Regarding the cooling, the SVD can be divided into two module categories, the Origami and edge-sensor modules (figure 2.8). Both require different cooling mechanisms due to the completely different APV25 placement. The APVs at the Origami modules are directly assembled on the sensor module, whereas the edge sensor APVs are mounted on hybrid boards at the forward and backward side of the detector, outside the active detecting region. In case of the chip-on-sensor design, the cooling can be realized with a common cooling tube, thermally connected to the readout chips. Figure 3.1 illustrates the cooling concept for the Origami sensor modules. To ensure safe and reliable operation, the tube must be attached to the detector module with proper clamps.

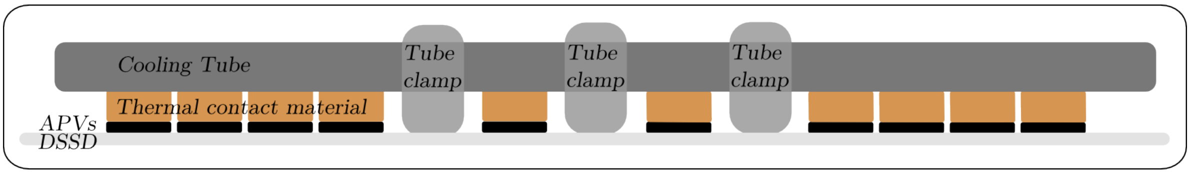

Figure 3.1: Schematic view of the Origami cooling concept shown here with one DSSD Origami sensor module, containing 10 APV25 chips.

The edge sensor APVs, assembled on hybrid boards will be cooled by cooling channels which are integrated in the end rings. Figure 3.2 depicts the structure of the end ring mounting and shows that APVs must be installed on both sides due to limited space. The APVs are separated into two hybrid boards which are installed back-to-back. Layer four, five and six needs four APV25 on the upper n side and six APVs on the lower p side whereas the layer three hybrid boards are assembled with six APVs on both sides. The mounting block is multifunctional, firstly it connects the ladder with the end rings, secondly it carries the hybrid board and thirdly it establishes the thermal contact between the cooled end rings and the lower APVs. The upper n side APVs from layer four, five and six are thermally contacted to the lower RO chips using numerous vias. For the cooling of the layer three APVs a heat pipe solution is envisaged and currently in draft status.

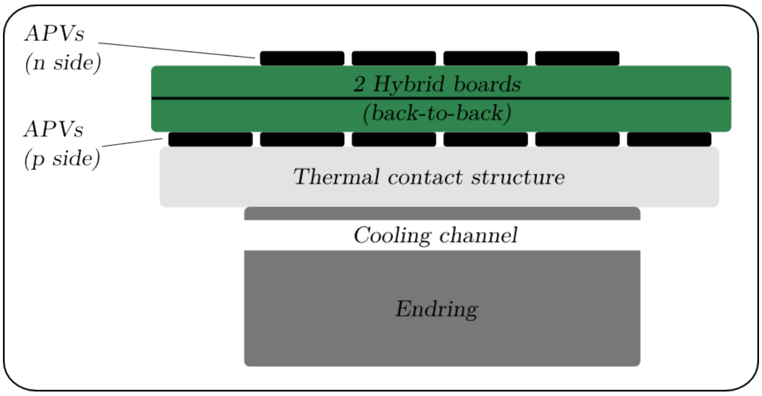

Figure 3.2: Schematic view of the hybrid cooling concept for layer four, five and six.

Comparing the two cooling concepts, it is quite obvious that the thermal transfer between the Origami APVs and the evaporation tubes is supposed to be much more efficient than the thermal transfer between the hybrid board APVs and the end rings. The Origami concept needs much less material between the APVs and the cooling tube than the hybrid cooling concept. This must be taken into account for the further development e.g. tube routing.

3.2 Material Budget

As already mentioned it is extremely important to keep the material budget as low as possible for good physics performance. Every component which is brought into the active region must be analyzed in detail concerning its radiation length.
Figure 3.3 illustrates multiple scattering of a charged particle in one scattering layer projected on a plane.

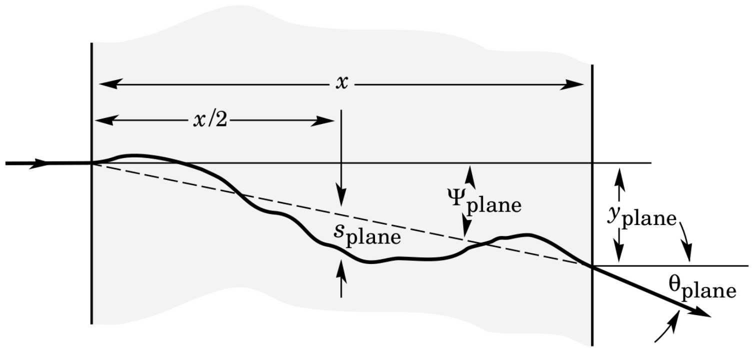

Figure 3.3: An illustration of the multiple Coulomb scattering of a charged particle in a scattering layer projected on a plane with its characteristic parameters. [15] modified

According to [16], the Coulomb scattering distribution represented by Molière's theory is almost Gaussian for small angles. If Θ_0 is defined as the variance of the projected deflection angle in the plane, the Gaussian approximation for the central 98% of the projected angular distribution has a width of Θ_0 as given in equation 3.2. In this equation, p is the particle momentum, βc its velocity, x is the thickness of the scatterer and X_0 the so called radiation length of the scattering material.

$$\Theta_0 = \Theta_{plane}^{rms} \tag{3.1}$$

$$\Theta_0 = \frac{13.6MeV}{\beta cp} z \sqrt{\frac{x}{X_0}} [1 + 0.038 ln(\frac{x}{X_0})] \tag{3.2}$$

The radiation length X_0 is a material constant, usually measured in gcm^{-2} but also often given in cm after dividing it by the materials mass density. The radiation length is defined by the distance, a high energy electron is traversing a material, reducing all but $\frac{1}{e}$ of its energy because of interactions by bremsstrahlung. It also means $\frac{7}{9}$ of the mean free path for pair production by a high energy photon. Tsai calculated and tabulated the values of L_{rad} and L'_{rad} for different materials, to calculate the radiation lengths with the equation 3.3 [17]. Here α is the fine-structure constant, r_e the classic electron radius, N_A the Avogadro's number, A and Z are the atomic mass and number of the scatterer/absorber and $f(Z)$ is an infinite sum which can be represented by $f(Z) = a^2[(1 + a^2)^{-1} + 0.20206 - 0.0369a^2 + 0.0083a^4 + 0.002a^6]$ for all elements up to uranium with $a = \alpha Z$.

$$\frac{1}{X_0} = 4\alpha {r_e}^2 \frac{N_A}{A} Z^2 [L_{rad} - f(Z)] + ZLrad' \tag{3.3}$$

If no experimentally determined data is available, the radiation length can also be calculated approximately with Dahl's analytic formula 3.4. According to the Physical Data Group [16], these calculated values coincide fairly well with Tsai's values.

$$X_0 = \frac{716.4}{Z(Z+1) ln \frac{287}{\sqrt{Z}}} gcm^{-2} \tag{3.4}$$

In many cases, not the radiation length of only one pure material is of special interest, usually the radiation length of different layers or composite materials is needed. Therefore, the radiation length has to be estimated from the radiation lengths of several different materials. The overall radiation length of composite materials can be estimated with the general formula given in equation 3.5.

$$\frac{1}{X_0} = \sum \frac{w_i}{X_i} \tag{3.5}$$

In equation 3.5, the individual radiation lengths are added proportionally, where X_0 is the radiation length of the composite material, X_i the radiation length of the individual composite i and w_i the fraction by weight for the i'th material in [g].

To compare different assembly materials, it is appropriate to give the different material slab thicknesses t_i in numbers N_i of their respective radiation length X_0 (equation 3.6).

$$N_i = \frac{t_i}{X_0} \tag{3.6}$$

The amount of material, which is crossed by a particle depends on the crossing angle. The shown calculation procedure however is assuming particles, traversing the material in perpendicular way to the material surface. Despite this assumption, different materials can be compared regarding their material budget.
For estimations of an inhomogeneous assembly it is often sufficient to calculate the average percentage of the material budget. This makes no statement about the spatial material distribution but allows comparisons of different structures. Therefore, the average material budget of each assembly component, relative to the whole assembly has to be figured out. To get this value, the calculated fraction N has to be multiplied by its assembly coverage C_i.

$$C_i = \frac{A_i}{A_0} \tag{3.7}$$

Term 3.7 calculates the ratio of the several component surface areas A_i and the whole assembly surface area A_0. The average material budget $\frac{X_i}{X_0}$ results from multiplying the assembly component coverage C_i with the number N_i of radiation lengths per component thickness.

$$\frac{X_i}{X_0} = N_i C_i = \frac{t_i}{X_0} \frac{A_i}{A_0} \tag{3.8}$$

3.3 Requirements

A lot of research and development is necessary to fulfill the requirements for a high precision particle detector. Cooling itself is only one small part of the entire project but also needs aplenty investigations in various domains. These domains include heat load, thermal contact, tubing, thermal insulation, material budget, refrigerant, installation and servicing as well as safety. Furthermore the usage inside a particle detector's acceptance region places high demands which cannot be taken for granted with commercially available cooling equipment. This section points out all important issues which must be considered when developing a proper cooling system.

3.3.1 General Requirements

General requirements can be applied to almost all of the mentioned domains and issues. They are subsequently listed and will not be further mentioned but can be provided for all requirements categories, mentioned in the following.

- Temperature-resistance down to cooling temperature
- Pressure-resistant tubing and components depending on the desired operation pressure
- Radiation hard coolant/materials inside the detector volume
- Chemical compatibility of components and coolant
- Corrosion-resistant tubes and components
- Long-term stability of materials

3.3.2 Heat Load

The overall thermal load of the SVD together with the PXD is about 970W. The PXD contributes $\sim$ 360W and the SVD $\sim$ 610W, where each APV25 has a power dissipation of 350mW. This requires a cooling system which is able to manage a total heat load of about 1kW. Although the SVD and PXD have a common cooling system, they can be considered as detached, because of individual evaporation circuits.
The main focus of this thesis lies on the SVD cooling, therefore the following requirements only apply to the SVD. Table 3.1 lists the APV count per ladder and the related heat loads. A division is made between the heat load resulting from Origami modules and hybrid boards.

Layer	**APVs Origami** #	**Heat load Origami** (W)	**APVs Hybrid** #	**Heat load Hybrid** (W)	**APVs Total** #	**Heat load Total** (W)
6	480	168	320	112	800	280
5	240	84	240	84	480	168
4	100	35	200	70	300	105
3	0	0	168	58.8	168	58.8
Sum	**820**	**287**	**928**	**324.8**	**1748**	**611.8**

Table 3.1: The SVD APV25 count and the corresponding thermal loads. [13]

3.3.3 Thermal Contact

To reach an adequate heat transfer from the RO chips to the cooling tube or mounting block, a proper thermal contact must be established. For both cooling mechanisms (hybrid board and Origami module), a proper application concept must be designed and thermally conductive material must be evaluated. The requirements for the heat contact are stated in the following listing.

- Thermal conductive materials with good thermal conductance in the material's propagation direction
- Electrically insulating material
- Similar thermal conditions at each APV
- Long-term temperature resistant materials (down to cooling temperature of -20°C)

The chip-on-sensor design of the Origami modules adds some requirements for the APV cooling, because the cooling tubes are located directly on top of the sensor modules, inside the active detector region.

- Minimal material budget
- Manageable assembly process on top of the sensor module/APVs
- Allowing tube remount
- Minimal stress on sensor during application/remount procedure

3.3.4 Tubing

The severely limited space requires an efficient pipe routing inside the detector volume. The same applies to tube connectors and fixing structures. To save space also at the tight supply channels, a cooling supply on both detector sides should be considered. This connection on both detector sides causes different transfer line lengths, leading to different heat losses. To ensure a proper heat load distribution, all these circumstances must be taken into account for the tubing design.

For efficient usage of the cooling system and the coolant, the evaporation tube routing must be divided into several parallel cooling sections with approximately similar heat loads. Several ladders can be cooled with a single pipe coil which is beneficial regarding space- and material budget. To save space inside the detector region, also specially designed miniature tube connectors are required.

The tubes must guarantee a trouble-free operation, without endangering functionality and safety, while allowing comfortable and easy handling at bending and assembling. This requires well dimensioned tubes and a well chosen chemically resistant material.

Another point which must be taken into account is the pressure drop along the tubes. The inner tube diameter must be chosen in a range where the pressure drop along the pipe remains at reasonable range.

Both, the tubes as well as the connectors must be electrically isolated at every single contact point from the detector components.
To avoid mechanical stress resulting from thermal expansions, the evaporation tubes are required to be float mounted on each ladder. The tubes must be assembled at the ladders with some kind of reclosable tube fixing structure, to ensure reassembling of tubes. This structure must be designed in such a manner, that mechanical stress to the sensor module is kept as low as possible during its assembling procedure because of the very fragile sensor structures.

3.3.5 Thermal Insulation

It is evident that a powerful cooling system also requires an efficient thermal insulation to prevent heat leaks and condensation. Condensate is dangerous because it can block mechanical components e.g. valves when freezing and in liquid state it can pose a serious risk to electronic parts. Not sufficiently insulated transfer lines cause heat leaks which could induce completely evaporated coolant, even before the cooling process takes place, especially with such a small coolant volume used in the detector.
Conventional tube insulation material can be considered because of sufficient space for the insulation of the evaporator transfer line path from the cooling plant to the outer boarder of the Belle II detector. The insulation concept for the path through service channels from the outer boarder of the Belle II detector to the SVD ladders is currently in draft status, for this field of application vacuum insulation is considered.
The detector concept envisages a cold gas flow through the detector volume which does not allow a vacuum insulation of the SVD itself. By continuously flushing cold nitrogen or dry air, condensation is prevented. Depending on the flush temperature, the total heat load can be decreased or increased. This additional heat load or cooling capacity must be taken into account for the evaporation tube dimensioning and mass flow calculations.

3.3.6 Material Budget

One of the most important figures of merit for the vertex detector is the amount of material seen by a particle, which is measured by the radiation length.
In the Belle II experiment relatively low momentum particles must be measured very well. At these low energies, Multiple Coulomb Scattering plays an important role in the vertex reconstruction of a particle. Regarding these circumstances, the detector design, including material selection, component design and usage, is strongly influenced and controlled by the material budget.
In case of a particle detector, the material budget is a significant value, indicating the transparency of the detector for the particles which should be detected. In order to keep the material budget as low as possible, all components have to be carefully selected and designed to avoid excessive amounts of material.
Cooling tubes are installed in the active region of the detector and therefore also count as material seen by the particles. To keep the cooling material as low as possible a

minimal tube diameter as well as a small wall thickness is needed. These very small and fragile components imply the need for a convenient and sophisticated mounting process of the tubes.
Beside the amount of material, the radiation length is important. Considerations must be carried out for each component, whether the material's radiation length or material amount is crucial. For better functionality it could sometimes be beneficial to even use materials with smaller radiation lengths but therefore in smaller quantities. For a proper detector cooling, the requirements for a sufficient heat transfer, together with minimal material budget must be considered.

3.3.7 Refrigerant

For an efficient cooling system, a coolant is required with optimally suited thermodynamic and chemical properties. A profound research was necessary to find the most convenient coolant for the SVD cooling. To state the requirements for the refrigerant, first the decision on the proper cooling system mechanism must be made.
Due to requirements of the readout electronics, the intended operation temperature of the APVs is -20°C. Furthermore, the coolant is required to be non-toxic, ensuring easy and safe installation, operation and maintainability. Also, the availability and disposal are issues which must be considered.

3.3.8 Installation and Servicing

During the design phase of the cooling system, including the cooling plant itself and all routing paths towards and within the detector, profound considerations about installation procedure and service feasibility is essential because of limited space. Furthermore the design must ensure reasonable access to other detector parts e.g. in case of malfunction.

3.3.9 Safety and Reliability

For an installation at the SVD a secure and reliable cooling system is inevitable. The SVD represents only one subdetector of the complex Belle II experiment, where any hazard must be reduced as far as possible. Hence, the material selection and dimensioning is one of the most important topics to ensure safe operation. Besides, safety devices such as interlocks and an extensive control system must be implemented to interfere in emergency cases.

3.4 Cooling System

To guarantee reasonable data taking, all APVs at the SVD shall operate at similar temperatures. The only working principle which ensures a constant temperature over long cooling tubes and multiple heat loads is a two-phase cooling system. This working principle is very efficient, because of the almost isothermal state change of the coolant at the phase change and optimally satisfies the requirements. It allows a small pressure drop during the evaporation process and does not induce significant temperature drops. This effect can even be minimized with a well chosen refrigerant.

The two-phase cooling principle is well established in the industrial refrigeration industry and becomes more and more utilized in particle physics. A well proven approach of a two-phase cooling is the Two Phase Accumulator Controlled Loop (2PACL) system [18, 19]. It is commonly used in capillary pumped loop systems, which were developed for satellite cooling [20]. The 2PACL cooling system was especially developed for detector cooling applications by NIKHEF. The thermal management of the LHCb-VELO[1] [18, 21] and the AMS-02[2] [22, 23] are implemented by liquid pumped 2PACL systems.

Figure 3.4 illustrates the 2PACL cooling system structure. The accumulator controls the evaporation pressure and hence the evaporation temperature of the cooling system. It is a pressure regulated vessel, containing a liquid/vapor coolant mixture. This filling is directly connected to the inlet of the condenser. The accumulator pressure is directly controlled by external cooling and heating, which respectively causes a pressure de- or increase. A cooling coil which is installed inside the upper vapor part of the accumulator volume and connected to an external chiller manages the cooling. The heating process is implemented by an electrical heater, located inside the liquid coolant at the bottom of the accumulator.

[1]The LHCb-VELO is a vertex detector specialized for B-physics, located at the Large Hadron Collider (LHC) at CERN.

[2]Alpha Magnetic Spectrometer-02, a particle detector performing measurements of cosmic rays with extremely high sensitivity, working as an external module on the International Space Station (ISS).

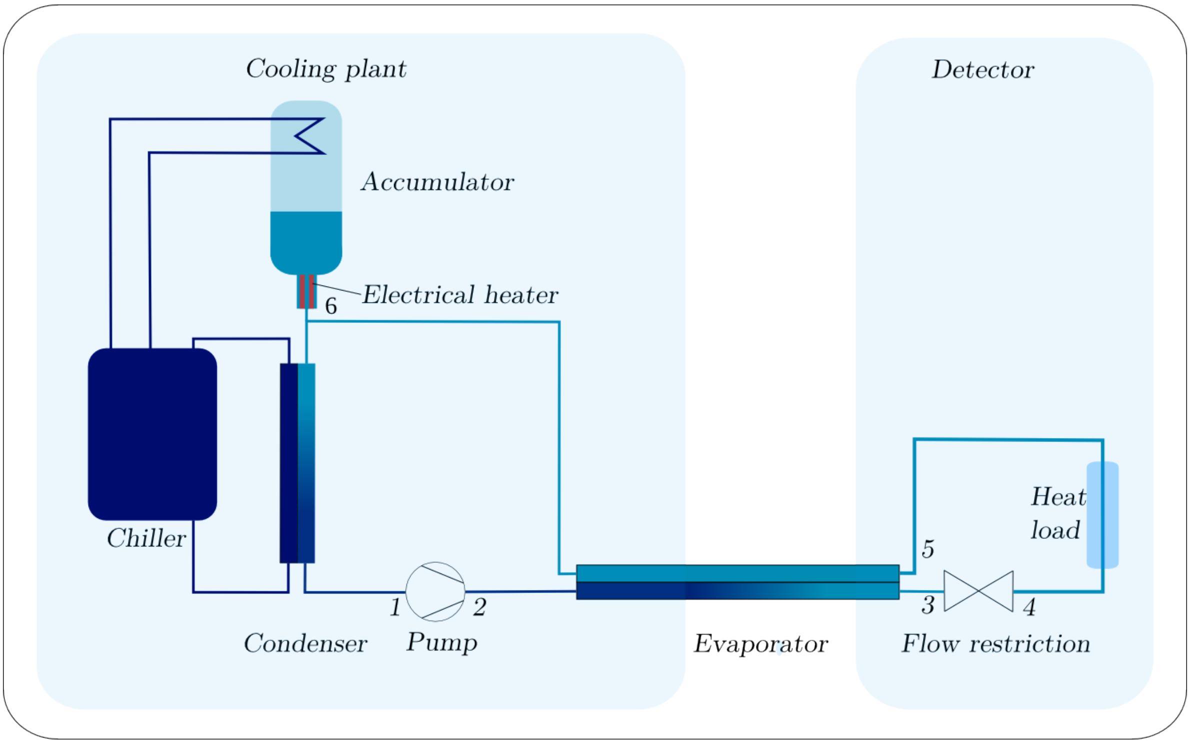

Figure 3.4: Schematic view of the 2PACL liquid pumped cooling system at the LHCb-Velo ([18] modified)

The sub-cooled liquid refrigerant is pumped (1-2) through the system. From node 2 to 3, the temperature of the sub-cooled liquid is raised in a heat exchanger to reach the saturation point at the desired evaporation pressure. The refrigerant mass flow is restricted (3-4) before the evaporation is induced by the detector heat load (4-5). The not completely evaporated liquid-vapor mixture is condensed (5-6) and sub-cooled (6-1) to ensure completely liquid pumping.
The main advantage of the 2PACL is that no active components are needed inside the extremely tightly packed and inaccessible detector area. The evaporator inside the detector area is a completely passive component. One problem, which often occurs at pumped two-phase systems, is the insufficient sub-cooling which may cause cavitation at pumping. The accumulator ensures cavitation free operation, because of an adjustable sub-cooling.

3.5 Refrigerant

Although the SVD cooling is a very special development, off-the-shelf components and a common coolant should be used. Cooling technologies are well developed and high-performance solutions are available, but nevertheless, the development and usage of coolants is still a big research field for the industry. The following paragraph resumes

the recent coolant development history, explaining why CO_2 will be used for the SVD cooling.
The targeted development of chemical refrigerants began in the early 20th century, with first attempts to replace the so called natural refrigerants due to their difficult handling. Natural refrigerants are:

- Not specially produced for cooling applications.
- A by-product in natural or chemical processes.

Although in the past the coolant efficiency was the most important criterion for the coolant choice, today also the environmental impact has become a major factor. In recent years, so called 'modern refrigerants' have been developed or in fact rediscovered due to environmental considerations. The values which characterize the environmental sustainability are the ozone depleting potential (ODP) and the global warming potential (GWP). Thermodynamic properties as well as safety, price, disposal and availability, still remain major criteria.
The first international environmental convention for protecting the ozone layer was the Montreal Protocol [24]. It restricted the usage of (H)CFCs[3] because of its big ozone depleting impact. The (H)CFCs were mainly used in air conditioning devices and as blowing gas.
(H)CFCs have been displaced subsequently by non ozone depleting (H)FCs[4]. These chemically quite similar compounds feature very similar thermodynamic properties and therefore existing technologies and facilities still could be used with only slight adjustments.
The insight of the strong greenhouse effect and long atmospheric dwell time of the (H)FCs resulted in an international environmental agreement, the UNFCCC [25] of the UNCED [26] in 1992. Its major intent was preventing dangerous anthropogenous disturbance of the climate system and slowing down the greenhouse effect as well as mitigating its consequences. The well known Kyoto Protocol [27], which became effective in 2005 actually reinforces the UNFCCC. The Kyoto Protocol is under international law, determining mandatory target values for greenhouse gas emissions in industrial counties, including fluorinated gases e.g. (H)FCs. This development finally has lead to a paradigm shift in refrigeration engineering. Consequently, the previously used greenhouse active (H)FCs were phased out, and completely new, less greenhouse active (H)FCs and other refrigerants have been developed. Besides, 'old' refrigerants which had already fallen into oblivion, were rediscovered. Due to the technological progress made in the twentieth century, natural refrigerants became manageable.
The most popular natural refrigerants are carbon dioxide, hydrocarbons and ammonia. Conventionally used (H)FCs have already been replaced in many cases by natural refrigerants. The biggest problems, in some cases, are high upgrade costs which can be compensated on the long term by lower operating costs, due to the higher efficiency of

[3] HCFCs and CFCs are Hydrochlorofluorocarbons and Chlorofluorocarbons, partly and fully halogenated Chlorofluorocarbons

[4] (H)FCs are partly and fully halogenated Fluorocarbons.

coolants and modern technologies.

The decision to use CO_2 for the SVD cooling had various reasons. 2PACL systems with CO_2 have already proven to be reliable for the detector cooling at the LHCb-VELO and the AMS-02. CO_2 cooling is a promising approach in particle physics because it combines excellent thermodynamic characteristics with a minimal overall material budget.

The two main decisive requirements for the SVD detector cooling which are satisfied by CO_2 were:

- Stable temperature conditions at the sensor modules.
- Minimal material budget in the active detector region.

The evaporation process theoretically takes place isothermally. Under real conditions a small pressure drop must be considered due to friction between coolant and tube wall. Consequently, this causes a decrease of temperature. Nevertheless, almost equal temperature conditions can be reached on every sensor module with the two-phase evaporative CO_2 cooling. To reach the desired evaporation temperature, the evaporation pressure of CO_2 is relatively high. CO_2 features a small pressure drop because of the relatively high operation pressure. It also provides high latent heat at the favored working pressure as well as its basically excellent thermodynamic properties, the good thermal conductivity and low viscosity:

- The more the refrigerant is compressed, the smaller the flowing velocity and therefore the lower the friction at the tube wall.
- Large latent heat and good thermal conductivity ensure low mass and low mass flow minimizing the friction.
- Low CO_2 viscosity also minimizes the coolants friction avoiding a large pressure drop along the evaporation tube.

Another big advantage of the high operation pressure is the small tube volume which minimizes the material budget. With CO_2 as coolant, much smaller tubes can be used compared to other coolants, e.g. water (used as coolant in the Belle I SVD).
Besides, there are a number of other reasons why CO_2 is an outstanding choice for detector cooling. It is non-toxic, non-flammable, non-corrosive and gaseous at atmospheric conditions which permits a safe and clean handling. Despite the high working pressure, operation is no danger because of the low refrigerant mass and thus limited stored energy. Moreover, CO_2 satisfies the required radiation hardness and the electrical isolation. It is available worldwide, cheap and an environmentally friendly natural refrigerant.
All these positive material properties of CO_2 together with the proven two-phase accumulator control technology promise an appropriate and smooth detector development and operation.

Chapter 4

The Open CO_2 Cooling System

A CO_2 cooling system was designed as a mobile test and development plant for sensor module cooling. The design must meet many functional requirements, but also stay as simple as possible. The most suitable design therefore is an open CO_2 cooling system, also called blow system.

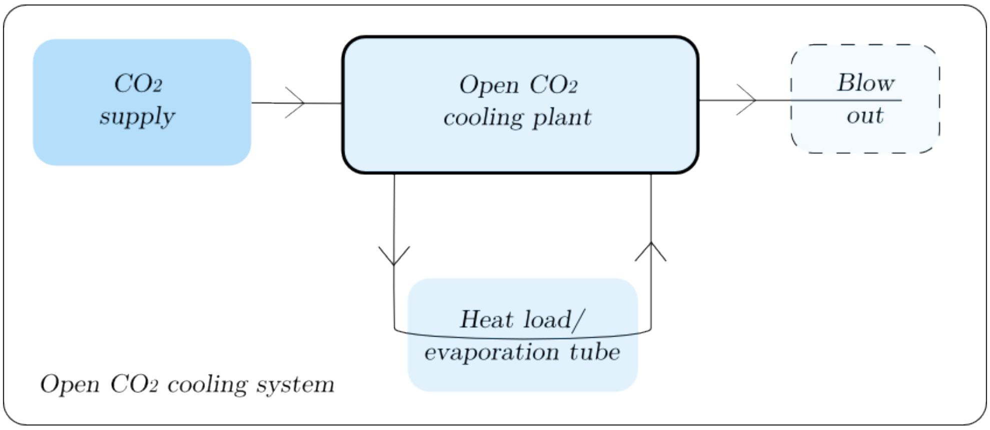

Figure 4.1: Schematic view of the open CO_2 cooling system.

Figure 4.1 shows the schematic setup of the system. The open CO_2 cooling system can be separated into a supply, the plant, an evaporation tube and a blowout. The cooling plant itself consists of active and passive pressure and mass flow regulation devices, various heat exchangers and electronics. The cooling plant is supplied with CO_2 which is blown through the cooling plant and after performing the cooling, vented into the environment.

This open CO_2 cooling system is based on research of the workgroups of H. Postema (CERN) and B. Verlaat (NIKHEF) who have been developing CO_2 cooling plants for particle physics detectors for many years. This chapter discusses the requirements, the functional principle, the component selection as well as the commissioning and operation of the cooling plant.

4.1 Motivation and Aims

In the course of the SVD development, a new cooling concept was required and the decision was made in favor of a CO_2-based cooling. The final SVD cooling is under development by a collaboration of MPI Munich, DESY, CERN and NIKHEF. This project is called IBBeLle and the developed cooling plant should be used for Atlas-IBL and Belle II. IBBeLle is still under development and its design derives from the MARCO (Multipurpose Apparatus for Research on CO_2) concept. The MARCO cooling plant is based on 2PACL as a basis for future detector cooling plants.
A small-scale test plant was necessary in order to evaluate SVD sensor modules which were developed and assembled at HEPHY and to become familiar with the new refrigerant CO_2. Based on this demand, an open CO_2 cooling system was designed and constructed. The development, realization and operation of the open CO_2 cooling system required design knowledge and tuning by experience. The blow system is used for developing and dimensioning of several cooling components and to test the new SVD sensor module cooling. Apart from the dedicated sensor module cooling e.g. at HEPHY or beam tests at CERN, another case of application is its usage for ladder tests at the ladder series-production. The implementation of the open CO_2 cooling system provides studies which are directly applicable to the SVD where the IBBeLle cooling plant will be used for the thermal management.

4.2 Requirements

The first step in developing the system was to figure out the requirements. The specifications have to comply with the SVD cooling requirements (chapter 3.3) but must be adapted to the dedicated use of the cooling plant at HEPHY. The detailed guidelines for the open CO_2 cooling system are listed below:

- The blow system is required to manage heat loads from 10W up to 1kW, for cooling tests in the research and test phase with one sensor module up to the overall SVD heat load.
- The CO_2 mass flow must be adjustable between $0.1gs^{-1}$ and $10gs^{-1}$ to manage the heat load. All components must be capable to handle this mass flow range.
- The cooling temperature is required to be -20°C. To reach this CO_2 evaporation temperature, a pressure of 20bar is needed.
- The blow system must be flexible enough for mass flow adjustments without time-consuming setup changes.
- All components on the high pressure side must withstand an operation pressure of 60bar which is around the CO_2 pressure in the supply bottle.
- The system must operate stably over several days to allow data taking under constant conditions.

- The cooling plant is required to be compact and transportable, such that it can be used for various applications at different locations.
- The operation of the blow system must be easy and reliable for convenient development, research and testing.
- Safety is a big issue inside the particle detector. Precautions have to be taken to ensure safe operation, e.g. installation of safety devices.
- To ensure a failsafe operation, all components must be tested individually and have sufficient safety factors.
- For a stable cooling system, all CO_2 traversed components must be dimensioned carefully. They have to be chosen adequately for the appropriate CO_2 state to avoid undesirable pressure drops.
- All CO_2 wetted materials must be chemical resistant.
- The tube coupling method must be easy, fast and resealable to perform adjustments in an acceptable time-frame.
- All components which are traversed by cold CO_2 must be thermally insulated to avoid condensation and heat leaks.
- An electronic control and monitoring system is required for an user-friendly operability.

4.3 Functional Principle

The two-phase evaporative cooling is a common cooling type widely used in industry. The following section reviews some basics from a thermodynamic point of view and leads over to the functional principle.

4.3.1 Application-Specific Basics

At the two-phase evaporative cooling, the latent heat of the coolant is used to dissipate the heat load. In an ideal process the power absorption of the coolant is equal to the dissipated power of the heat source, which is not exactly the case in a real system.
The specific latent heat L is called the amount of energy in form of heat Q, which is absorbed or released by a thermodynamic system of the mass m during its first order phase change at constant temperature (equation 4.1). The molecular structure of a substance is the reason for the isothermal phase change. The whole supplied amount of heat is used for changing the molecules potential energy, completely without affecting the kinetic energy in terms of temperature changes.

$$L = \frac{Q}{m} \tag{4.1}$$

Generally, the enthalpy H is the total energy of a thermodynamic system. It is also often used in form of the specific enthalpy h, where the enthalpy H is referred to the mass m of the system. The relation between the amount of heat Q, provided to a thermodynamic system and the thereby induced change of the specific enthalpy Δh is given in equation 4.2. The mass flow rate $\dot{m}$ and the thermal output $\dot{Q}$ are meaningful parameters in the refrigeration technology. Equation 4.3 shows the correlation between $\dot{Q}$, $\dot{m}$ and Δh. In order to ensure complete absorption of the thermal output $\dot{Q}$ by the evaporating CO_2, the mass flow $\dot{m}$ has to be properly dimensioned.

$$Q = m\,\Delta h \tag{4.2}$$

$$\dot{Q} = \dot{m}\,\Delta h \tag{4.3}$$

4.3.2 Pressure Enthalpy Diagram of CO_2

The pressure-enthalpy diagram (p-h diagram) of the particular refrigerant is an indispensable tool in the design process of a cooling system. It provides the designer with vital data, e.g. pressure, temperature, enthalpy and phase state under certain conditions.
The temperature of CO_2 cannot be changed directly; a temperature change can only be initiated implicitly by changing enthalpy or pressure. The enthalpy is changed by adding or releasing energy to/from the system, the pressure can be changed by expansion and compression of the coolant.
Figure 4.2 shows the p-h diagram of CO_2 with some highlighted marks. The points represent special states and the lines specific transitions which can be directly assigned to the cooling process. The thick, black lines are isotherms at -20°C and 20°C. The blue- and red-colored lines denote the saturation which is divided into a liquid and gaseous section, respectively. Beyond the left-hand side of the saturation line, the CO_2 is liquid and beyond the right-hand side, it is gaseous. Beneath the saturation line, the CO_2 prevails in a two-phase mixture. The amount of gaseous fraction is proportionally given from 0 to 1, with 1 meaning fully evaporated, gaseous CO_2. The isotherms and states at constant density are marked with thin black lines.

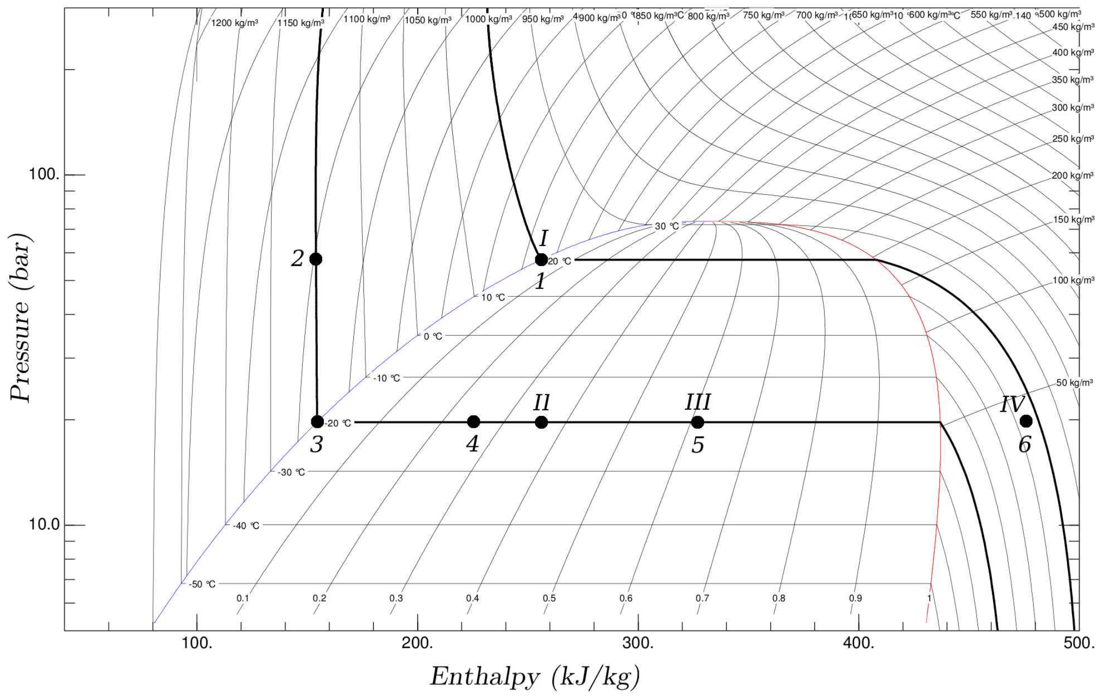

Figure 4.2: The pressure-enthalpy diagram for an open CO_2 system. See text for description.

4.3.3 The Pressure-Enthalpy Diagram for an Open CO_2 Cooling System

This section describes the functional working principle of the open CO_2 cooling system by means of the p-h diagram. The p-h diagram 4.2 is supplemented with marks to describe the process. The Roman numerals describe the blow system without sub-cooling and the Arabic numerals represent the developed open CO_2 system including sub-cooling.

To describe the principle function of an evaporative blow system, a case study was chosen with an assumed evaporation pressure of 20bar. The following description for the fluid behavior is idealized and the given pressure and temperature values are rounded.

- **I** : Initial state; fully liquid CO_2 at 57bar and 20°C (room temperature).
- **I→II** : Expansion; the pressure is reduced to 20bar to reach the desired evaporation temperature.
- **II** : Two-phase mixture at 20bar and -20°C.
- **II→III** : Cooling; the enthalpy change Δh is driven by an external heat load. The p-h diagram shows that at the beginning of the cooling (II) the CO_2 is already partly gaseous. It can also be seen that the usable evaporation enthalpy is just a fraction of the overall evaporation enthalpy.
- **III** : Partly evaporated CO_2 at 20bar and -20°C. Here the cooling of the heat load is finished but there is still evaporation enthalpy left.
- **III→IV**: Heating; absorption of the remaining evaporation enthalpy and heating to prevent the outlet from jamming by freezing humidity.
- **IV** : Finished; the completely evaporated and heated CO_2 at a temperature above the dew point.

In order to improve its efficiency, the blow system is extended by a sub-cooling unit. This significantly increases the usable amount of evaporation enthalpy. The corresponding steps are described in the following.

- **1** : Initial state; fully liquid CO_2 at 57bar and 20°C (identical to I).
- **1→2** : The liquid CO_2 is sub-cooled by 4→5 which reduces the temperature.
- **2** : Sub-cooled liquid CO_2 at 57bar and -20°C (compare to II).
- **2→3** : The pressure is reduced to reach the desired evaporation pressure at the saturation line.
- **3** : Fully liquid CO_2 at 20bar and -20°C.
- **3→4** : Cooling; the evaporation and therefore the heat absorption starts from fully liquid state at the saturation line (compare to II→III).
- **4** : Partly evaporated CO_2 at 20bar and -20°C.
- **4→5** : Sub-cooling; the remaining evaporation enthalpy is used for the sub-cooling of the incoming CO_2, where the enthalpy difference between 1-2 and 4-5 is in principle the same.
- **5** : Partly evaporated CO_2 at 20bar and -20°C.
- **5→6** : Heating; absorption of the remaining evaporation enthalpy and heating to prevent the outlet from jamming by freezing humidity.
- **6** : Finished; completely evaporated and heated CO_2 at a temperature above the dew point.

The main benefit of the sub-cooling is that point II is shifted to the left along the isotherm on the saturation line to point 3. This optimization makes it possible to use the entire evaporation enthalpy and therefore saves coolant mass.

4.3.4 CO_2 Evaporation Behavior

At this point it is important to mention that the evaporation process has a massive impact on the heat conductivity of the cooling pipe and coolant. Gases are much less heat conductive than liquids and the flow conditions also affect the heat conductivity. These circumstances must be taken into account when the CO_2 starts boiling.
Depending on the CO_2 saturation rate, various flow patterns appear due to bubble formation. CO_2 expands up to the tube surface, thereby disturbing the thermal conductivity. The cooling capacity disappears even before the liquid CO_2 is completely evaporated because the tube wall effectively gets insulated by the gas. This phenomenon is called dry-out and generally limits the heat absorption capacity.
Under certain conditions, however, the flow boiling process is beneficial for the heat transfer. In the beginning of the flow boiling process, the heat dissipation benefits from convection due to turbulences in the coolant. This effect occurs at liquid-vapor qualities with a high liquid ratio. Figure 4.3 shows the principle of flow boiling in horizontal tubes. The blue line denotes the fluid temperature and the cyan line the tube temperature. It should be noted, that in practice the evaporation inside the tube is not isothermal due to the tube wall friction, causing pressure drop. The illustration shows that the temperature difference between the evaporating coolant and the tube wall is not constant in the dry-out zone. At that certain liquid-vapor quality (dry-out point), the thermal resistance and hence the tube wall temperature increases rapidly. This dry-out phenomenon strongly limits the maximum cooling power and must be taken into account when calculating the mass flow. The heat conductivity mainly depends on the fluid flow pattern, the heat flux, the evaporation temperature and slightly on the mass flow. All these effects have been well investigated and described by different groups [18, 28, 29].

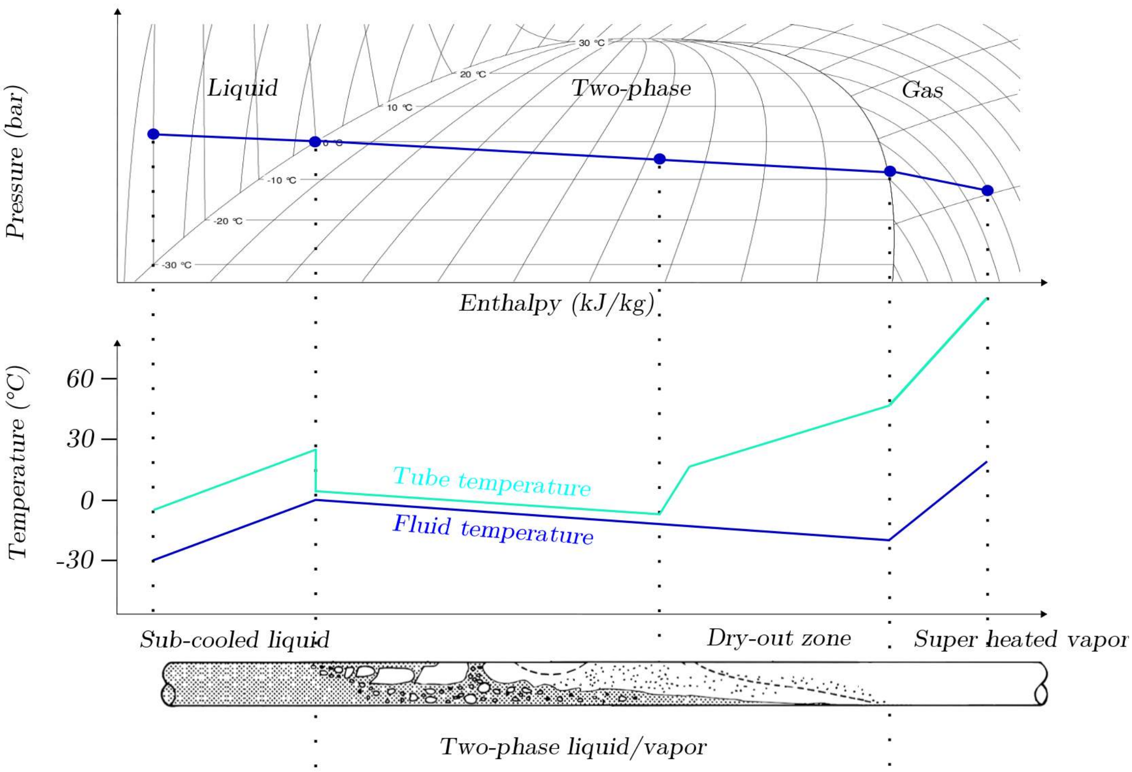

Figure 4.3: The principle of flow boiling in horizontal tubes with different flow patterns. ([18, 30] modified)

The heat transfer coefficient and pressure drop along the evaporation tube depends on the tube dimensions. According to [28], the SVD evaporation tubes can be classified as minichannels. Details of the flow boiling process in minichannels have been investigated by [28] and [29].

4.4 Schematics

The theoretically described processes with reference to the CO_2 p-h diagram must be implemented by the appropriate components. Several actuators are needed to control and regulate the process. Moreover, many measuring devices are necessary for monitoring the process data. Figure 4.4 shows the schematic view of the open CO_2 cooling system with all its components and measuring devices.

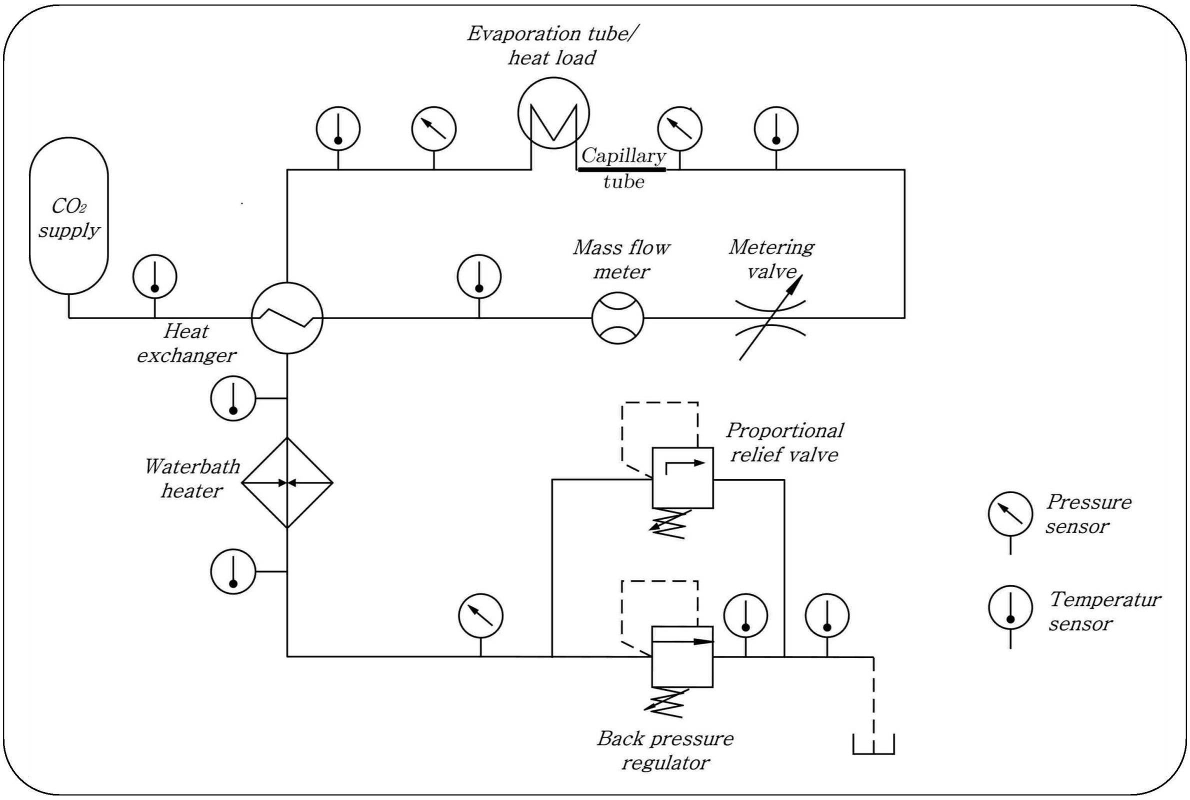

Figure 4.4: Schematic view of the open CO_2 cooling system.

The liquid CO_2 is usually stored in a cylinder and extracted by a plunger tube to ensure liquid withdrawal. The pressure of the CO_2 in the cylinder (~60bar at ambient temperature) blows the liquid into the cooling system. The incoming liquid CO_2 from the reservoir is sub-cooled in a heat exchanger by using the remaining evaporation enthalpy after the cooling process. Then the mass flow is measured with a mass flow meter and set with a metering valve. A capillary tube is installed directly before the evaporation tube to reduce the pressure and reach the required evaporation pressure. After passing the evaporation tube, the remaining evaporation enthalpy of the not yet fully evaporated CO_2 is used for sub-cooling the CO_2 from the inlet. The heat exchanger is followed by a water bath heater to fully evaporate the used CO_2 and heat it up above the dew point. A back pressure regulator is installed at the end of the system, to ensure a constant system pressure at the blow system. To avoid a damaging overpressure in the system, a proportional relief valve is installed in parallel to the back pressure regulator as a safety device. After the back pressure regulator the used CO_2 is vented into the environment.

4.5 Component Selection

All functional blocks from the schematics must be implemented using adequate components. In this section, the chosen components will be presented with their properties, considering all requirements from section 4.2.
Particle detector cooling is not in scope of the refrigeration industry because industrial-sized plants usually have completely different requirements, e.g. much higher cooling capacities. One major issue of this thesis is to benefit from industrial experience and to reach a maximum of quality and reliability by using well developed and technically mature components. The availability of commercial off-the-shelf components which are compatible with CO_2 benefits from the worldwide advance of industrial CO_2 cooling plants. The challenge is to get an overview of the huge market and to adapt standard components to very special and sometimes even contradictory needs. The development of new components cannot be justified due to high costs and long development cycles. Therefore, standard components must be used wherever possible.

4.5.1 General Comments

In the dimensioning of the various components there is a certain hierarchy in the decisions to be made, starting with the requirements and dimensioning of the evaporation tubes. All effects caused by components must be considered already at their dimensioning. One effect with massive side impacts is a diameter change which comes along with a change in pressure and mass flow. Almost every component in a cooling system is affected by this phenomenon. In contrast to the theoretical descriptions in sections 4.3 and 4.4, the ideal state changes cannot be put into practice with real components. The metering valve is a good example to illustrate this problem. The mass flow throttling by diameter reduction is accompanied by a significant pressure drop at the valve, depending on the reduction scale. The inverted effect occurs at the capillary tube. This component is intended to reduce the pressure due to its diameter change, but it also causes a flow reduction.
Beside the desired control and operation range of the components the material decision is a big issue. The most qualified material for CO_2 traversed components is stainless steel rather than aluminum or plastics due to non-corrosion and strength. Stainless steel has an excellent material resistance against CO_2. The most preferred stainless steel family is AISI 316 also known as 1.4401 because it is not prone to corrosion. Among the AISI 316 steel series, the AISI 316L (1.4404) steel is favored due to its low carbon content, resulting in a higher corrosion resistivity.
Many components are available in metric and imperial dimensions which would call for a decision in favor of either standard. However, a consistent usage of only one standard is hardly feasible because not all used components are available in both types.
A big issue which also has to be kept in mind when selecting components is that components must be installed without the danger of trapping cold liquid. Every volume needs a relief to avoid damaging pressures.

4.5.2 Tubing

In order to find the most suitable tube dimension for the various usages, investigations regarding the material and tubing must be carried out. When considering the tubing design, the necessary thermal tube insulation also has to be taken into account.
The following different tube types were chosen for the open CO_2 cooling system.

- **Stainless steel tubes** – stiff, relatively small bending radius, cheap
- **Pure stainless steel hoses** – flexible, relatively large bending radius, extremely expensive
- **PTFE hoses with stainless steel jacket** – flexible, relatively large bending radius, expensive, limited chemical and material resistance
- **Pure PTFE hoses** – highly flexible, relatively small bending radius, cheap, limited chemical resistance, highly restricted material resistance

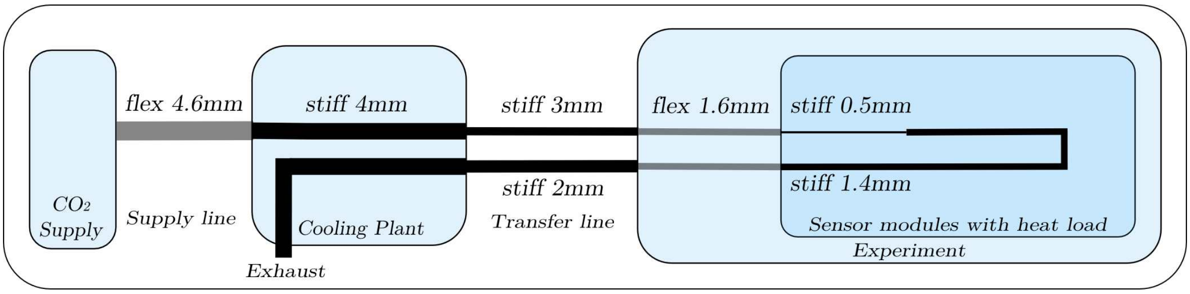

Figure 4.5: Overview of the different tube dimensions, used at the open CO_2 cooling system. The given dimensions are the inner diameter of the tubes. The gray lines indicate flexible tubes and the black lines show stiff tubes.

Different application fields require different tubing types; the dedicated tubing type and dimension is chosen depending on the fluid state and space conditions (figure 4.5). The tube selection is described in the following paragraphs and is mostly based on experience and trial-and-error.

Supply line: CO_2 supply – cooling plant

The CO_2 reservoir, usually a single gas cylinder, is connected to the cooling plant with a 1m long flexible hose. The PTFE hose, reinforced with a stainless steel jacket withstands pressures up to 155bar at -53°C. The inner tube diameter was chosen to be 4.6mm, in order to be consistent with the tubing inside the cooling plant.

Tubes inside the cooling plant

Seamless stainless steel tubes (AISI 316L) with 6mm outer diameter and 4mm inner diameter are chosen for all tubes inside the cooling plant. These tubes are bent with 15mm radius using a special tube bending device. The operating pressure range of these tubes vary depending on the manufacturing method but can be assumed to be at least 400bar.

Transfer line: cooling plant – experiment – cooling plant

The evaporation tube is not directly connected to the cooling plant. The experimental setup usually is installed approximately 10m away from the cooling plant. Due to the evaporation process, the return line is chosen with a bigger diameter than the liquid-only feed line to provide more volume for the (partly) vaporized CO_2. The feed line has 2mm inner diameter and the return line 3mm, both with 0.5mm wall thickness.

Tubes inside the experimental setup

Depending on the usage, several kinds of tubes are installed in the experimental setups. One special issue and big problem occurs if the heat load with the evaporation tube must be moveable within limited space conditions. In this case only plastic tubes can be used because of their high flexibility and high bending capabilities. Nevertheless, plastic tubes should be avoided whenever possible and only used at non-critical and easily accessible locations because of their limited durability, especially when combining high pressure and low temperatures. Regular checks and replacements are inevitable to assure a reliable operation.

Evaporation tube

The evaporation tube dimensions strongly depend on the SVD cooling requirements. As discussed in 3.5, CO_2 together with the 2PACL allows very small tube sizes. For cooling tests with the open CO_2 cooling system, tube dimensions similar to the planned SVD tube dimensions are used.
First considerations proposed an evaporation tube wall thickness of 0.05mm. After pressure, bending and assembly tests, this proposal was discarded because of the very complicated handling of such fragile pipes. Based on these experiences and calculations, the SVD evaporation tube is currently dimensioned with 0.1mm wall thickness, 1.4mm inner diameter and made of stainless steel. Tubes with 0.1mm wall thickness cannot be used together with conventional ferrule tube fittings and also the tube bending requires expert experience. Tubes with 0.2mm and 0.3mm wall thickness were applied for easier handling during the development phase and tests with the open CO_2 cooling system. Figure 4.6 gives a comparison of several tested and planned evaporation tube diameters.

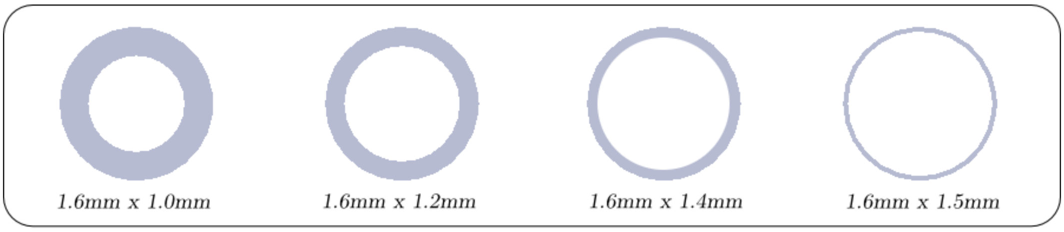

Figure 4.6: Outer and inner diameters of the different evaporation tube dimensions.

4.5.3 Capillary Tube

A capillary tube is a common expansion and refrigerant control device which reduces the pressure due to friction at the tube wall, usually deployed in small-sized refrigeration plants. It is a relatively long and narrow tube, with a very small diameter compared to the evaporator. In contrast to an active adjustable expansion device such as a pressure reduction valve, a capillary tube is a passive device with constant length and orifice. Capillary tubes are obviously much simpler and cheaper than active expansion devices. The absence of an active part also has the advantage that there are no parts which can be worn out and no service is required. However, this component cannot be adjusted in case of requirement changes.
In an open cooling system, the expansion device is placed before the evaporator to bring the CO_2 in saturation. Theoretically, the evaporation process aiming at reaching the desired evaporation pressure is performed by an adiabatic expansion.
A capillary tube is indeed a simple device but its effects are quite complex. Besides the pressure reduction from the condenser pressure to the evaporation pressure, the capillary tube also regulates the mass flow. The state of the CO_2 flowing through the tube can differ between a sub-cooled liquid and a partly evaporated two-phase fluid, depending on the tube dimensioning. The adiabatic capillary tube model has been under consideration since 1940. Since then, the capillary characteristics have been widely studied and different analytic solution methods were developed. An approximate analytic solution of adiabatic capillary tube dimensioning is given by [31].
The capillary dimension for the open CO_2 cooling plant was found by trial-and-error. The trial-and-error approach is best practice and most common for determining the most suitable capillary tube length, because many details cannot be accurately considered in calculations. For the open CO_2 cooling system a capillary tube with about 200mm length and 0.5mm inner diameter was figured out to be the most appropriate. This is relatively short but in combination with all other assembled components and their pressure drops, this is sufficient in order to reach the required evaporation pressure.

4.5.4 Fittings

Different methods are available for connecting tubes, valves and other components. The most common tube coupling methods are screwing, welding and soldering. Depending on the usage and space conditions, all of these methods are used in the plant. Reusable

and resealable screwing connectors are favored in most cases because frequent modifications were inevitable during the development of the plant.
Screw-mountable ferrule tube fittings are commonly used in industry. There is a broad market for this type of connecting mechanism, offering different materials and a lot of different configurations and sizes including adapters to other common threaded connectors. Swagelok [32] provides fluid system solutions including fittings, valves and regulators. Swagelok ferrule tube fittings were chosen for the blow system. The structure and working principle of these fittings are shown in the following figures 4.7 and 4.8.

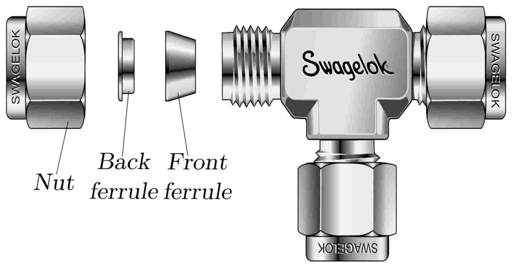

Figure 4.7: Assembly parts of a ferrule tube fitting.
[32]

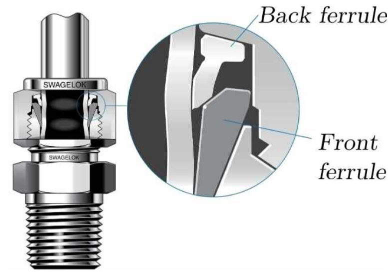

Figure 4.8: The ferrule tube fitting clamping mechanism.
[32]

This fitting design is live-loaded with two ferrules per connection, one back ferrule and one front ferrule. The two ferrules allow the separation of the sealing and the tube gripping function. The front ferrule is driven into the tube and the fitting body, establishing a primary sealing between the tube and the fitting body (figure 4.8). The back ferrule simultaneously hinges inwards creating a strong radial grip on the tube.
One major advantage of this ferrule tube fitting design is that no torque is transmitted to the tubing during the installation process. This enables tube connections even with very small and fragile tube dimensions. It also allows gas-tight resealability which is necessary for a research plant. The full specified pressure resistance of these conventional tube fittings is guaranteed for wall thicknesses down to 0.2mm. For thinner tube walls, special fittings with less clamping force need to be designed or other connecting mechanisms like soldering or welding must be used. These ferrule tube fittings also qualify for connecting plastic tubes. In this case support sleeves are used for soft hoses to guarantee a good sealing.

4.5.5 Valves

The most significant factor when selecting valves is the control range. For the open CO_2 cooling plant, the mass flow and pressure must be adjustable over a wide range because various experiment demands have to be fulfilled. Thus, a compromise has to be found between covering the whole desired control range and enabling fine adjustments at specific values.

The flow coefficient[1] is a parameter commonly used for valve dimensioning and comparison. This relative measure indicates the flow efficiency of a fluid through a valve by giving the relation of the pressure drop in the valve and the corresponding fluid flow rate. The metric flow coefficient K_V is given in m^3h^{-1}, in US units it is denoted C_V and given in gpm. C_V is by definition the number of US gallons per minute of water which flows through a valve with a given opening degree and a pressure drop of 1psi. K_V is similarly defined as the volumetric flow in m^3 per hour of water through a valve with a given opening degree and a pressure drop of 1bar. To convert K_V into C_V and vice versa, a factor must be multiplied due to the differing units (equation 4.6).

$$K_V = q_V \sqrt{\frac{\Delta p_{(K_V)}}{\Delta p} \frac{\rho}{\rho_0}} \tag{4.4}$$

$$K_V = \frac{q_V}{259.5 p_1} \sqrt{\rho T_1} \tag{4.5}$$

$$K_V = 0.86 C_V \tag{4.6}$$

The above mentioned equations 4.4 and 4.5 ([33, 34]) are chosen for two special use cases which are described in the following sections. Equation 4.4 can be applied for valve sizing at liquid flow conditions. Equation 4.5 must be used for gas flow situations with the following conditions $p_2 < \frac{p_1}{2}$ where p_1 and p_2 are the pressures before and after the valve, measured in bar. $\Delta p_{(K_V)}$ is the static pressure drop of 1bar and $\Delta p = p_1 - p_2$ is the static pressure drop along the valve in the corresponding unit bar. ρ_0 stands for the specific fluid mass of water in kgm^{-3}, ρ is the specific mass of the chosen fluid in kgm^{-3} and q_V is the volumetric flow rate given in m^3h^{-1}. T_1 is the gas temperature before the valve in °C.

Metering valve

Metering valves are used to control gas and liquid flow rates and are usually designed as needle valves. The requirements for the metering valve are described in detail below:

- Mass flow regulation $0.1 gs^{-1}$ – $10 gs^{-1}$
- Manage liquid and gaseous flow
- Operation pressure 60bar
- Maximum permissible pressure drop at the valve 25bar
- Operation temperature -20°C

[1] This characteristic value was introduced by Masoneilan Company in 1944 for the first time and has become a standard for valve designing (DIN EN 60534).

- CO_2 resistant material
- Electrically controllable

In order to estimate the valve size, the flow coefficient which depends on the mass flow regulation and the limited pressure drop must be calculated. The pressure drop values used for calculations with equation 4.4 are assumed based on experience, but the results should be taken just as guide values. The choice of realistic values can be only made after gaining experience in this application area. A common issue is the estimation of safety factors, ensuring adjustments within the control range. In this context, it is important to note that too many tolerances can result in greatly oversized valves where the required range cannot be controlled as accurately as desired.
For estimating the appropriate valve size, the smallest and largest flow coefficients $K_{V_{min}}$ and $K_{V_{max}}$ are calculated with equation 4.4 to gain an overview about the required flow coefficient range. The smallest flow coefficient can be calculated with the smallest mass flow rate and the biggest pressure drop at the valve. The largest flow coefficient is calculated correspondingly. The CO_2 is usually liquid at the location where the metering valve is installed, hence equation 4.4 applies. The following values are used for the calculation:

Density of water at 1.0bar	ρ_0	$=$	$998.6 \mathrm{kgm}^{-3}$
Density of sub-cooled liquid CO_2 at 20.0bar	ρ	$\sim$	$1000 \mathrm{kgm}^{-3}$
Minimum volumetric CO_2-flow	$q_{V_{min}}$	$=$	$0.1 \mathrm{gs}^{-1}$
Maximum volumetric CO_2-flow	$q_{V_{max}}$	$=$	$10.0 \mathrm{gs}^{-1}$
Minimal pressure drop in the valve	Δp_{min}	$=$	1.0bar
Maximal pressure drop in the valve	Δp_{max}	$=$	25.0bar

The results for $K_{V_{min}}$ and $K_{V_{max}}$ calculated with the above-noted values are:

$$K_{V_{min}}=7.2\ 10^{-5}\ \mathrm{m}^3\mathrm{h}^{-1}$$
$$K_{V_{max}}=3.6\ 10^{-2}\ \mathrm{m}^3\mathrm{h}^{-1}$$

One single metering valve is not able to manage such a wide range. Two needle valves with different flow coefficients, stem tapers and orifices were chosen to cover the whole required mass flow range. The corresponding valve properties are listed in table 4.1.

	S Series	31 Series
Body	316 stainless steel	316 stainless steel
Sealing	fluorocarbon FKM O-ring	metal to metal
$\mathbf{K_V}$ ($m^{-3}h^{-1}$)	0.003	0.03
Orifice (mm)	0.81	1.6
Maximum working pressure (bar)	137	344
Working temperature (°C)	-23 to 204	-53 to 37
Stem taper (°)	1	2

Table 4.1: Properties of two used metering valves form Swagelok [32].

The chosen metering valves are depicted in figure 4.9 and 4.10. On the left hand side is the S series low-flow metering valve and on the right hand side the medium-flow valve from the 31 series. The major differences between these two valves are the stem taper and the orifice size, both resulting in different flow coefficients and a fine adjustability. The smaller the taper of the stem and the longer the stem, the finer the possible flow adjustment and vice versa. Concerning the orifice, it can be said the larger the orifice the smaller the pressure drop and the higher the flow coefficient which also pertains conversely.

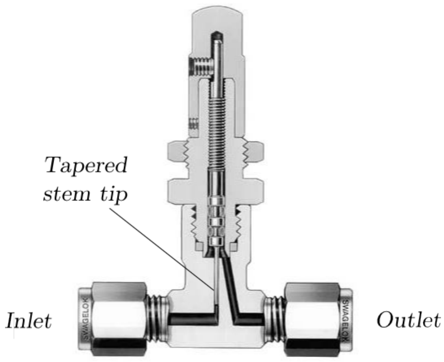

Figure 4.9: Metering valve of the S series.

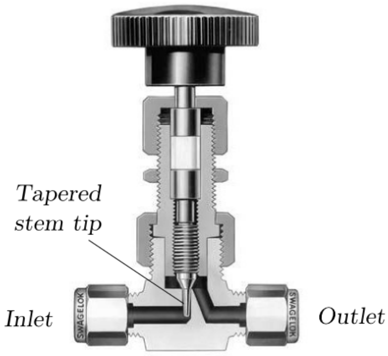

Figure 4.10: Metering valve of the 31 series.

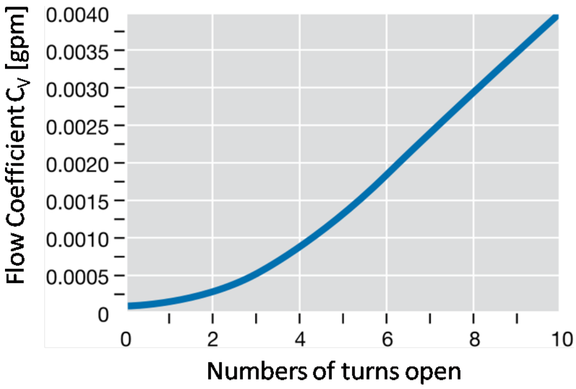

Figure 4.11: Flow coefficient diagram of the S series metering valve.

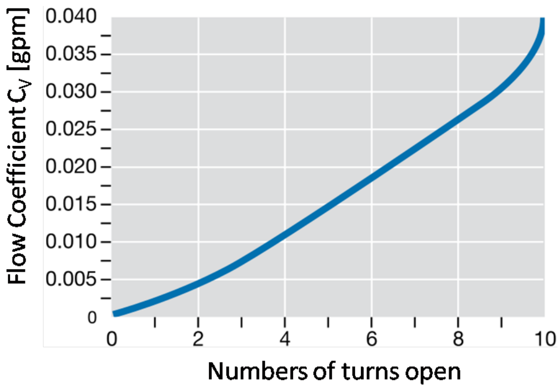

Figure 4.12: Flow coefficient diagram of the 31 series metering valve.

Figures 4.11 and 4.12, respectively, show the valves' flow coefficients depending on the opening rate. These diagrams make clear that the S series valve should be used for fine adjustments at very low mass flow conditions.
A low mass flow is required for most test setups where only few detector modules with a low overall heat load are operated. Experiment results confirm that the series S valve is a good choice for the most common mass flow range between 0.5 and 2gs^{-1}.
Both selected valves can be equipped with the same electrical actuator, enabling remote and automated control.

Pressure regulator

Another type of valve which is necessary for the cooling system is a pressure regulator. Basically, there are two different construction types of pressure regulators. On the one hand, there are regulators with a piston sensing mechanism and secondly regulators with a diaphragm mechanism. Piston sensing regulators are used for pressures which are more than ten times higher than the required pressures at the blow system. Diaphragm-based regulators are sufficient for this cooling application and also much cheaper.
The specific type of the needed pressure regulator is a so called back pressure regulator which controls the pressure on the upstream side. According to the cooling plant layout (figure 4.4), the back pressure regulator is located at the back end of the system to ensure the required evaporation pressure.
Equation 4.5 is used for the pressure regulator dimensioning. p_1 is required to be 20bar, p_2 is assumed to be 6bar and the volumetric mass flow is also assumed with 10gs^{-1}. The gaseous CO_2 directly before the back pressure valve is heated up to about 20°C and therefore has a density of ρ=41 kgm^{-3}. The result of the K$_V$-calculation is K$_V$=0.02m^{3}h^{-1}.
Again, Swagelok offers an acceptable valve in its product line. The chosen back pressure regulator (type KBP) is rather oversized but its K$_V$ still fits best compared to other valves with a similar control range. To ensure fine pressure adjustability, the control

range of the valve should not only cover the required pressure range, it must almost match the needed pressure range. Despite the relatively high flow coefficient, it was successfully tested even for mass flow rates down to $0.5gs^{-1}$. The back pressure regulator KBP is depicted in figure 4.13.

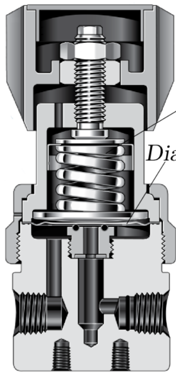

Figure 4.13: The KBP back pressure regulator from Swagelok with the flow direction from the left hand side towards the right hand side.
[32]

The working principle of this regulator is described as follows. The inlet pressure is controlled by balancing an adjustable spring force against the force of the inlet pressure. The convoluted and non-perforated metal diaphragm (Alloy D-750) is highly sensitive and the metal-to-metal diaphragm seal minimizes potential leakages. The maximum inlet pressure of the regulator is equal to its pressure control range which is given with 0.68 to 34.4bar. The flow coefficient of the chosen KBP back pressure regulator is K_V=$0.17m^3h^{-1}$. The valve body is made of stainless steel (AISI 316). The fluid contacting sealing PCTFE[2] features a good chemical resistance against CO_2 and is thermally stable down to less than -250°C [35].

Proportional relief valve

A proportional relief valve is also installed in the blow system but it has a different functional principle and properties compared to the back pressure regulator. In the blow system, it is applied as a safety valve to avoid a damaging overpressure on the low pressure side of the cooling plant. As described in section 4.4, the proportional relief valve is placed in parallel to the back pressure regulator. The functioning principle of the proportional relief valve is based on a spring which builds up a mechanical counter pressure against the fluid pressure. The degree of the opening can be adjusted by varying the preload of the spring.

[2] PCTFE is the abbreviation for Polychlorotrifluoroethylene, a thermoplastic chlorofluoropolymer $(CF_2CClF)_n$

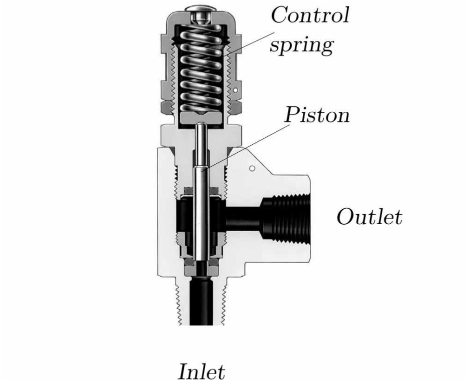

Figure 4.14: The proportional relief valve from the Swagelok's R3A series. [32]

The chosen proportional relief valve is out of the R3A series again from Swagelok. It is depicted in figure 4.14. To avoid destruction of the back pressure regulator, the pressure on the low pressure side must not exceed 34.4bar. The chosen proportional relief valve must be able to manage negative temperatures down to -20°C. Usually the fluid temperatures at the relief valve are much higher than -20°C but technical problems can never be excluded and therefore the worst case scenario must be considered. This low temperature valve has a neoprene O-ring sealing with a working temperature range down to -23°. It is able to manage pressures up to about 400bar. The relief pressure range can be modified by different spring kits. The installed spring kit allows a pressure range adjustment between 24.1 and 51.7bar and is set to 28bar relief pressure. The set pressure is repeatable within ±5% at room temperature according to the manufacturer's data.

4.5.6 Heat Exchanger

One of the most difficult issues in selecting cooling components was to find an appropriate heat exchanger which is applicable for the required pressure and mass flow range. In contrast to all other used components, heat exchangers are exclusively used in cooling/heating devices and are therefore only available for specific cooling applications. Pressure ratings exceeding 50bar are treated as high pressure ranges on the heat exchanger market. CO_2 and its relatively high pressure range is a rather new concept in the refrigeration technology. Heat exchangers used with common refrigerants are designed for much lower pressure ranges. CO_2 became popular in the recent years and with this development, especially heat exchangers have to be redesigned or even constructed from scratch.
An efficient heat exchanger has to be made out of a thermally well conductive material and it is essential to have big contact surfaces between the chambers of the two media to ensure thorough thermal coupling. Copper and aluminum are popular heat exchanger materials with a good thermal conductivity but cannot be used for the open CO_2 cooling system. Both are not suitable because either of high corrosion in combination with

CO_2 and/or their low mechanical strength to withstand high pressures. A reliable CO_2 system requires a stainless steel heat exchanger.
In general, many different heat exchanger construction types like rib or honeycomb structures are common. Heat exchangers based on coils are also very popular. The two types which qualify for the application in the open CO_2 cooling system are the plate heat exchanger design and the concentric tube heat exchanger design. Finally, a plate heat exchanger was chosen because of its much smaller dimensions. Plate heat exchangers vary in their flow direction and are basically available in two different types. The concurrent flow and the counter current flow design, where the counter flow design is able to exchange more heat than the concurrent flow type because of the higher mean temperature difference along the heat contact surface. The temperature along the heat transfer surface is location-dependent. If the temperature profile along the transfer face is not known, the heat transfer $\dot{Q}$ in W can be estimated with the following heat transfer equation 4.7 by assuming a mean temperature difference $\Delta\Theta$.

$$\dot{Q} = kA\Delta\Theta \tag{4.7}$$

$$\Delta\Theta = \frac{\Delta T_1 - \Delta T_2}{ln(\frac{\Delta T_1}{\Delta T_2})} \tag{4.8}$$

In these equations, k is the heat transfer coefficient given in $Wm^{-2}K^{-1}$, A is the heat transfer surface in m^2 and $\Delta\Theta$ the mean temperature difference in K. The mean temperature difference results from the fluid temperature differences ΔT_1 at the inlet and ΔT_2 at the outlet of the heat exchanger in K.
Equation 4.7 does not consider a possible change of the fluid phase. In case of the open CO_2 cooling system, the CO_2 changes its phase during the evaporation inside the heat exchanger and this circumstance must be considered for dimensioning. In reality, the heat transfer coefficient k is not constant during the evaporation process. [36] describes a method to calculate a mean heat transfer coefficient by considering the changing liquid/vapor mixture. Its different values depending on the varying liquid/vapor quality have to be integrated over the whole evaporation/condensation line.

One of the global leaders in designing plate heat exchangers is SWEP [37]. In the past, the rarely offered high pressure plate heat exchangers were reinforced by heavy, expensive and complex external and internal frames to withstand high operation pressures. The new frameless, high pressure double wall technology no longer requires reinforcement. With this new design, heat exchangers withstand relatively high pressure ratings and can be produced in a much more compact and lightweight implementation. Figures 4.15 and 4.16 show the newly designed heat exchanger B9 in comparison to an old plate heat exchanger with heavy steel reinforcement. During the blow system development phase, the B9 heat exchanger was available only as a fully functional prototype.

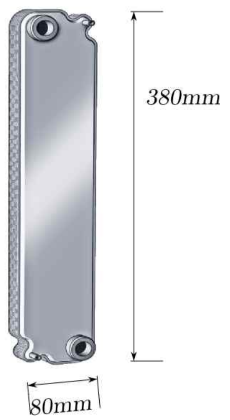

Figure 4.15: The newly developed B9 brazed plate heat exchanger from SWEP with the latest frameless, high pressure double wall technology
[37]

Figure 4.16: A reinforced high pressure brazed plate heat exchanger with heavy steel reinforcement of the B16DWU series from SWEP.
[37]

The B9 heat exchanger by SWEP has been specially developed to operate with super-critical CO_2 on the high pressure side at up to 140bar and water on the low pressure side with 48bar. These ratings allow safe operation of the heat exchanger in the open CO_2 cooling system. The whole heat exchanger is made from stainless steel AISI 316. Its performance is scalable by varying the number of plates. For this application, four plates are brazed together with pure copper. Because of the originally super-critical gas cooler design, the water side has quite big connectors. In order to avoid too much expansion volume in the system, these connectors were adapted. The flow directions of the fluid were chosen to be in opposite directions to ensure the most efficient heat exchange.

4.5.7 Water Bath Heater

Various very complex effects (chapter 4.3.4) prevent the usage of the entire evaporation enthalpy in a two-phase cooling system. Therefore, the phase with mostly liquid fluid is used for cooling the effective heat load. The remaining evaporation enthalpy of the not entirely evaporated CO_2 must be dissipated to avoid jamming of the exhaust with dry ice. This is managed in an additional heat exchanger, the water bath heater. It consists of a pipe coil immersed in electrically heated water. Figure 4.17 shows the water bath heater containing the CO_2 traversed stainless steel coil. Two heating cartridges are mounted on the base plate inside the tube spiral and are controlled by a thermostat. An electrically driven stirrer inside the tube coil avoids a temperature gradient of the heated water by convection.

Figure 4.17: The water bath heater with a tube spiral, a stirrer and two heating cartridges. The side walls are not shown. The filling volume of the water bath heater is about 4l.

The evaporation spiral in the water bath is bent from the same stainless steel tube that is used in the cooling plant, with 4mm inner diameter. Due to limited space, the spiral is as small as possible but still able to dissipate the maximal amount of evaporation enthalpy.
The water bath heater must have enough power to evaporate the whole CO_2, even without any heat load. The enthalpy difference Δh which must be dissipated is composed as follows:

	Total CO_2 evaporation enthalpy at -20°C
-	Amount of enthalpy for the sub-cooling
+	Amount of enthalpy for overheating to reach positive temperatures above the dew point
	Total enthalpy difference which must be dissipated

The maximal assumed CO_2 mass flow for the cooling plant is 10gs^{-1} with a maximal available Δh of 250kJgk^{-1}, resulting in a maximal cooling capacity of 2500W. The spiral length can be calculated with the heat transfer surface A by using the equations 4.3 and 4.7. Again, the heat transfer coefficient of the CO_2 is not constant during the evaporation and the method described in [36] is used to calculate a mean heat transfer coefficient. This results in a calculated spiral tube length requirement of 3.2m. Adding some margin, the assembled spiral in the open CO_2 cooling system is 3.5m.

4.5.8 Thermal Insulation

The thermal insulation of all components which are traversed and contacted by cold CO_2 is a very important issue. The two main reasons are to avoid heat leaks and to

prevent frozen ice outside of the components. Heat leaks and the omnipresent environmental heat load can have a big impact on the overall heat load if they are not kept as low as possible. This must be taken into account in the mass flow calculation. The insulation should be considered already during the tubing geometry design; complicated tube geometries which prevent a vapor tight insulation should be avoided.
Investigations have shown that an insulation foam is sufficient for the application in the open CO_2 cooling system. After some considerations the common AC/Armaflex from Armacell [38] was chosen. It is available in different styles and layer thicknesses. AC/Armaflex is a high-performance and flexible elastomeric foam insulation material featuring a closed cell structure to prevent wicking of moisture. Its low heat conductivity of $0.038 \mathrm{Wm^{-1}K^{-1}}$ ensures a good thermal insulation against the environment. It also fulfills the safety requirements because it is self-extinguishing, does not dip and does not spread flames. Besides its technical advantages, the installation procedure is easy and convenient when the tubing design geometry is kept simple.
The manufacturer specifies the minimal insulation layer thickness to be about 6mm in order to avoid condensation with AC/Armaflex at a fluid temperature of -20°C and an environment at room temperature and a relative humidity of 40%. In order to also minimize the heat losses due to poor insulation, a thicker insulation foam is chosen. Wherever the tubing geometry and the space conditions allow it, a 9mm thick AC/Armaflex layer is installed.

4.5.9 Mass Flow Meter

For the monitoring of process data like pressure, temperature and mass flow, electronic sensors are installed at strategic points of the blow system. To measure the mass flow, various devices with different functional principles have been investigated. Having a closer look on the requirements and the circumstances, it becomes clear that the coolant can exist in a mixed phase state at the measurement location. This occurs when the subcooling does not work properly and the CO_2 already starts evaporating before passing the measuring location. This circumstance limits the choice of an appropriate device. A common indirect approach to get the mass flow is to measure the volume flow and to calculate the mass flow by multiplying with the density. This approach cannot be used for this application because there is no information about the current CO_2 density at the time of measuring. With a Coriolis mass flow meter however, the mass of a liquid or gaseous medium or even a mixture of both can be measured independently of the phase state. The internal structure of the Coriolis mass flow meter is shown in figure 4.18.

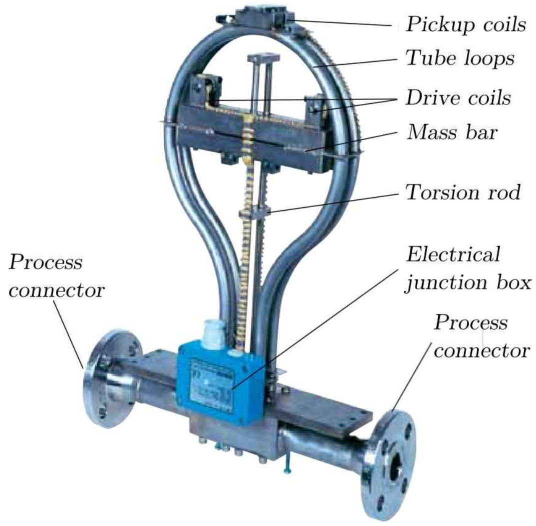

Figure 4.18: The internal structure of a Coriolis mass flow meter. [39]

The mass flow meter basically consists of two parallel Omega-shaped tubes where the overall flow is separated equally to both tubes. The tubes are stimulated by an actuator to perform small vibrations, symmetrically in opposed directions around the tube basis. The oscillating system is driven by two mass cross bars, mounted on vertical torsion rods. The tube traversing fluid will pass a range of different velocities along the way due to the tube vibrations. This leads to a Coriolis force generation, causing a bending in the top of the tube. This deflection is measured as a phase shift between the two tubes. The whole mechanism is symmetrical, but mirror-inverted for both tubes to increase this effect. The phase shift directly relates to the mass flow which passes the tube. If the fluid does not flow through the tubes, they oscillate symmetrically without any phase difference. Due to the Coriolis principle, the mass flow through the tube can be measured directly independent of its density.

The chosen mass flow meter Rheonik RHM 03 [39] is part of the low flow series, equipped with a flow transmitter (Rheonik RHE 14 [39]), meeting all requirements set in 4.2. It has a measuring range from $0.6gs^{-1}$ up to $83gs^{-1}$, a temperature rating from -45°C to 210°C and a pressure rating of up to 150bar. The housing is made of stainless steel AISI 304, the measuring loops are AISI 904L and the process connectors are AISI 316Ti. The mass flow meter is powered by a supply voltage between 8 and 28V. The output signal is a current loop between 4 and 20mA, proportional to the measured mass flow.

4.5.10 Temperature Sensors

The measurement of the fluid temperature is a major issue to control and regulate the proper function of the cooling. It can be directly measured by thermocouples inside

the fluid flow or indirectly by reconstruction based on tube wall temperatures. Tube wall temperature values are important because it can be assumed that this temperature is equal to the temperature of the RO chips in the SVD. The tube wall temperature can also be used to calculate the coolant temperature by considering the heat transfer coefficient of the tube wall material.
The tube wall measurement is mostly performed because it is easy, flexible and cheap. The sensor positions can be easily changed wherever needed, depending on the particular measurement setup without affecting the plant operation. For the tube wall temperature measurement, two different sensors were chosen and tested, a k-type thermocouple and a digital temperature sensor DS620 from Maxim [40]. Figures 4.19 and 4.20 shows the digital temperature sensor and the thermocouple, both assembled on a stainless steel pipe.

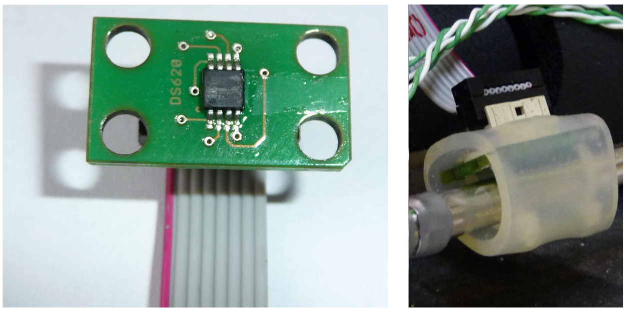

Figure 4.19: Digital temperature sensor DS620 assembled on a tube (6mm outer diameter).

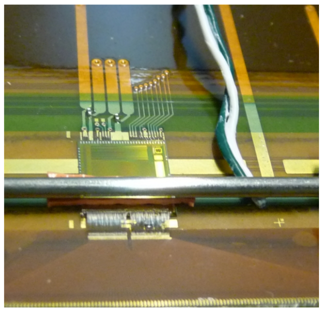

Figure 4.20: Thermo element k-type assembled below the evaporation tube (1.6mm outer diameter).

4.5.11 Pressure Sensors

In contrast to the temperature sensors which can easily be mounted outside the liquid flow, the pressure sensors have to be placed inside the fluid flow. This fluid touching component also requires CO_2 resistance in addition to an adequate temperature range. The chosen AKS2050 pressure transmitter from Danfoss [41] has a CO_2 contact area out of stainless steel AISI 316L. This pressure transmitter is a relative metering device which provides the pressure in relation to a constant reference pressure. The measurable pressure ranges from -1 to 59bar and the maximum operation pressure is 100bar. The temperature range is between -40°C and 85°C. The supply voltage of the pressure transmitter is 4.75 to 8V. The output signal is linear and ratiometric from 10-90% of the supply voltage. Three pressure sensors are assembled in the cooling plant at strategic points (section 4.3), one of this is shown in figure 4.21.

Figure 4.21: An assembled pressure transmitter AKS 2050 (Danfoss).

4.5.12 Control Electronics

The open CO_2 cooling plant with all its components is quite a complex system which has to be monitored and controlled. For this purpose, a computer-aided control unit is indispensable. The cooling system is designed to work as a stand-alone device hence a rather powerful computer is needed.
The decision was made in favor of the Alix3d3 single board computer from PC Engines [42] (figure 4.22). An additional expansion board was required to connect all previously mentioned sensors. It connects all different temperature, pressure and mass flow sensors and also features a multifunctional display and push buttons. The board runs Ubuntu and a server which provides all data over Ethernet. The counter part of the embedded PC which receives all data is a standard desktop PC running a LabVIEW program (National Instruments). The whole electronics and software development was done by the HEPHY electronics department. The following pictures show the embedded PC itself, the expansion board and the display.

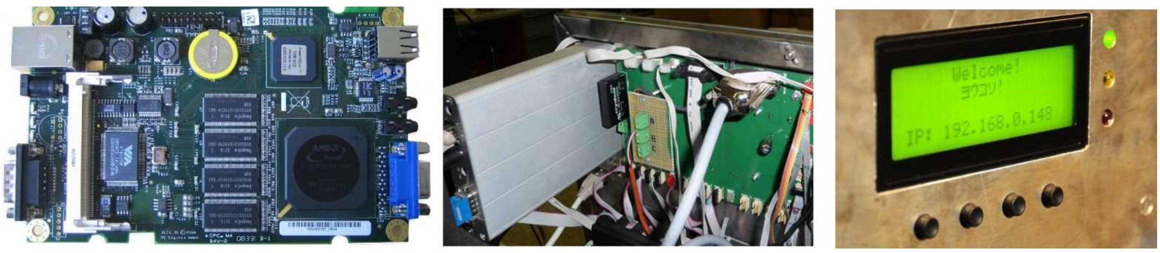

Figure 4.22: Alix3d3 single board computer, expansion board and display.
[42]

4.6 Assembly and Commissioning

One major goal of this project was to develop a portable cooling plant which can easily be operated. The outline dimensions of the cooling plant are 460mm $\times$ 460mm $\times$ 550mm (width $\times$ height $\times$ depth). This box has 4 CO_2 connectors, one for the CO_2 supply, one for the exhaust and two connectors back and forth to the evaporation tube. In an extensive CAD design phase the whole plant was designed and the tube routing and component positioning optimized. Figure 4.23 shows the CAD design of the cooling plant and the completely assembled cooling plant with all components.

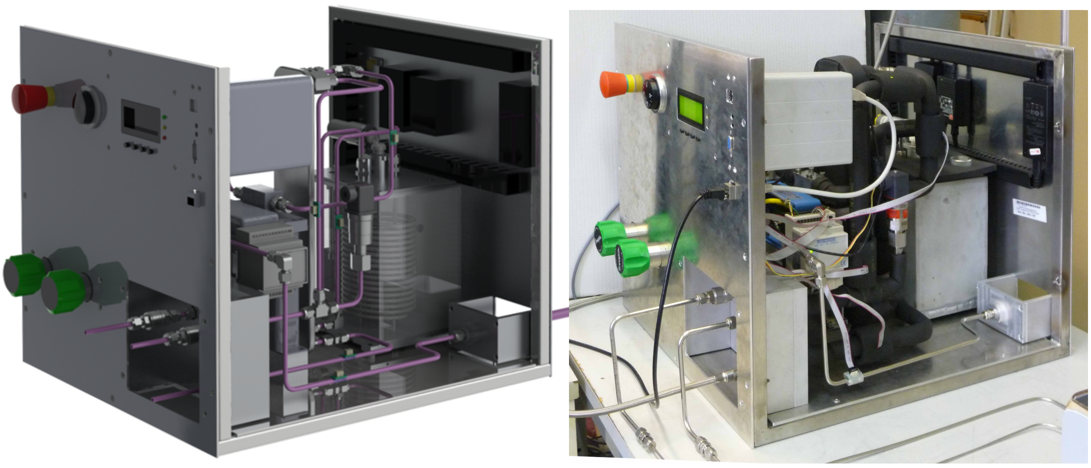

Figure 4.23: The 3D CAD design of the open CO_2 cooling plant and the fully assembled cooling box.

The framework of the box is made out of welded stainless steel square tubes. All control elements and ports are integrated in the front side panel of the box to simplify the usage. All components are attached at the front, bottom or back walls to ensure easy maintenance. Due to the convenient arrangement, each component is easily reachable. For safe transportation, the open sides are covered to protect the components inside the box.

Figure 4.24 shows the first prototype evaporation tube for the commissioning of the cooling plant, a stainless steel AISI 316 tube with 2mm inner diameter. This dimension is slightly bigger than the planned SVD evaporation tube, but it was chosen because of its easy handling. The U-shaped evaporation tube was equipped with dummy heat loads and temperature sensors.

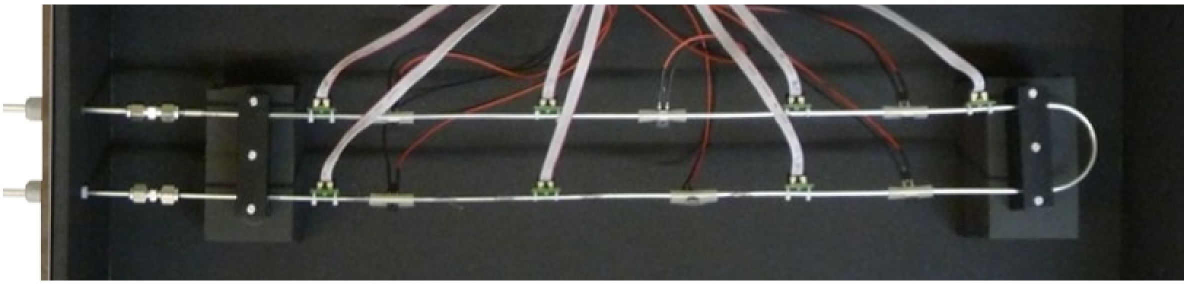

Figure 4.24: Evaporation tube setup for the first tests at HEPHY with assembled temperature sensors and dummy heat load.

Due to the intensive and careful preparation, the commissioning and first tests required a certain time but went smoothly straight away. Subsequently, the electronics and the LabVIEW interface were developed and commissioned. After a few months of familiarization and bug fixing the blow system and the refrigerant were fully operational. The next step was to prepare and adjust the system for sensor module prototype cooling. The dissipated heat load per sensor is about 3.5W. Therefore, a relatively low mass flow was sufficient and the low flow metering valve was installed.
Origami sensor module prototypes had already been assembled and tested at HEPHY previously but without evaporative CO_2 cooling. Several Origami sensor module prototypes were updated with cooling tubes and connectors to be able to combine several evaporation tubes of serially connected sensor modules. This test setup was very similar to the planed SVD barrel ladder cooling concept (compare section 3.1). Precise details of the cooling tube assembly are given in chapter 5. Sensor module prototypes consisting of one and two DSSDs were assembled with evaporation tubes and tested with the open CO_2 cooling plant to verify the designated Origami cooling concept. Figure 4.25 shows a DSSD module prototype with one DSSD and an assembled cooling tube on top of the APVs.

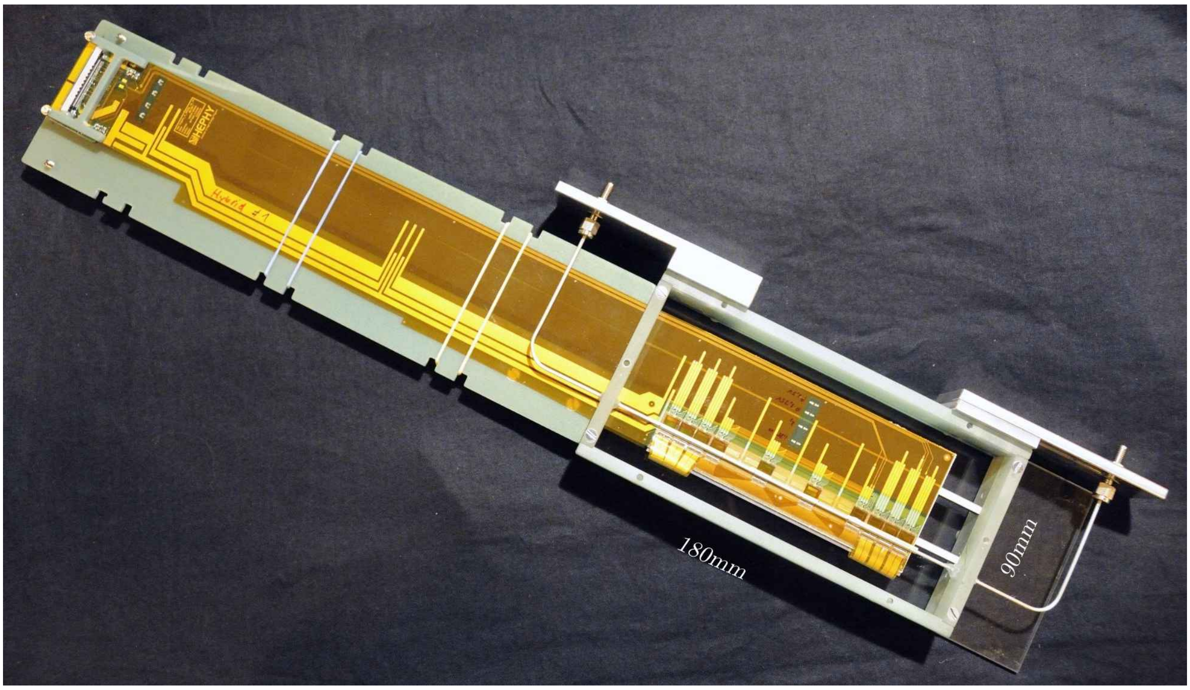

Figure 4.25: Prototype of an Origami DSSD assembled with an evaporation tube for cooling tests. The module frame dimensions are 180mm × 90mm and the assembled evaporation tube has a length of about 400mm.

4.7 Operation

The open CO_2 cooling plant has been tested in several short- and long-term runs and found to function perfectly. First, it was used at HEPHY laboratories to test sensor module prototypes with cooling and to evaluate various tube attachment concepts and designs (chapter 5). It also operated reliably in several long-term beam tests at CERN with only minor issues. More application details and measurement results are given in the following paragraphs.

4.7.1 Test Setup

The test setups usually do not vary significantly. The biggest differences are the length of the connection tube between the cooling plant and the evaporation tube and the varying heat loads. Figure 4.26 shows the beam test setup with the open CO_2 blow system. The cooling plant is an independent entity, separated from the sensor module. It is connected on one side to the CO_2 supply and on the other side to the experimental setup.

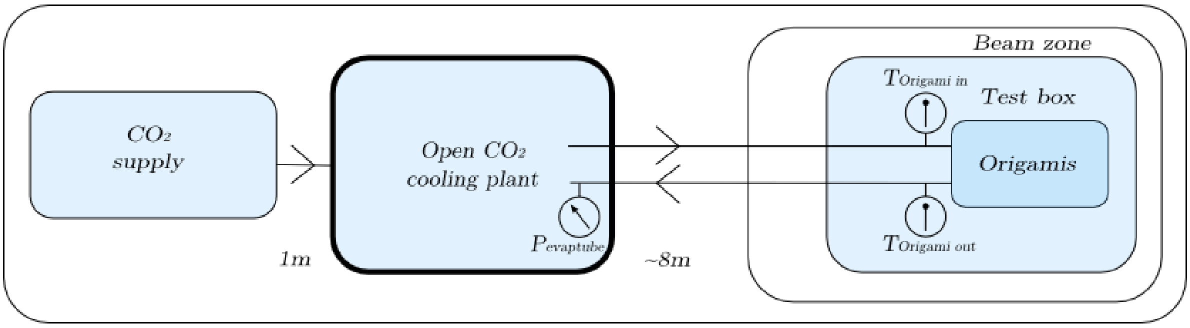

Figure 4.26: Schematic view of the cooling plant setup at the beam test (CERN).

Figure 4.27 depicts the actual test setup at CERN (North Area, SPS secondary beam line H6). The open CO_2 cooling plant and the CO_2 supply were located outside of the beam zone. The CO_2 supply was ensured by a battery of 12 CO_2 cylinders with a total capacity of 480kg. This huge amount of coolant was enough to ensure a continuous operation over roughly 5 days.

The sensor modules were installed in a test box (figure 4.28) which was operated in the particle beam. The particle beam provided 120GeV hadrons. This light-tight test box was equipped with a moveable sensor module mounting table, a scintillator and a photomultiplier. To avoid condensation and icing on the detector components, the test box was continuously flushed with nitrogen at about 20°C. This nitrogen flow represents an additional environmental heat load for the evaporation tube which is not thermally insulated (figure 4.25). This additional heat load is significant and has to be considered when adjusting the mass flow.

In this setup, three Origami modules with a total APV power dissipation of 10.5W were cooled by using a mass flow of $0.9 gs^{-1}$. When assuming an evaporation enthalpy of $100 kJkg^{-1}$, only $0.1 gs^{-1}$ would be sufficient to dissipate the 10.5W. Due to the relatively high environmental temperature, the heat leak of the non-insulated evaporation tube represents the largest part of the heat load. Therefore, the mass flow has to be an order of magnitude higher. The mass flow adjustment was done by using the dry-out point as a reference point. With this trial-and-error method, $0.9 gs^{-1}$ was found to be the lowest mass flow just avoiding dry-out.

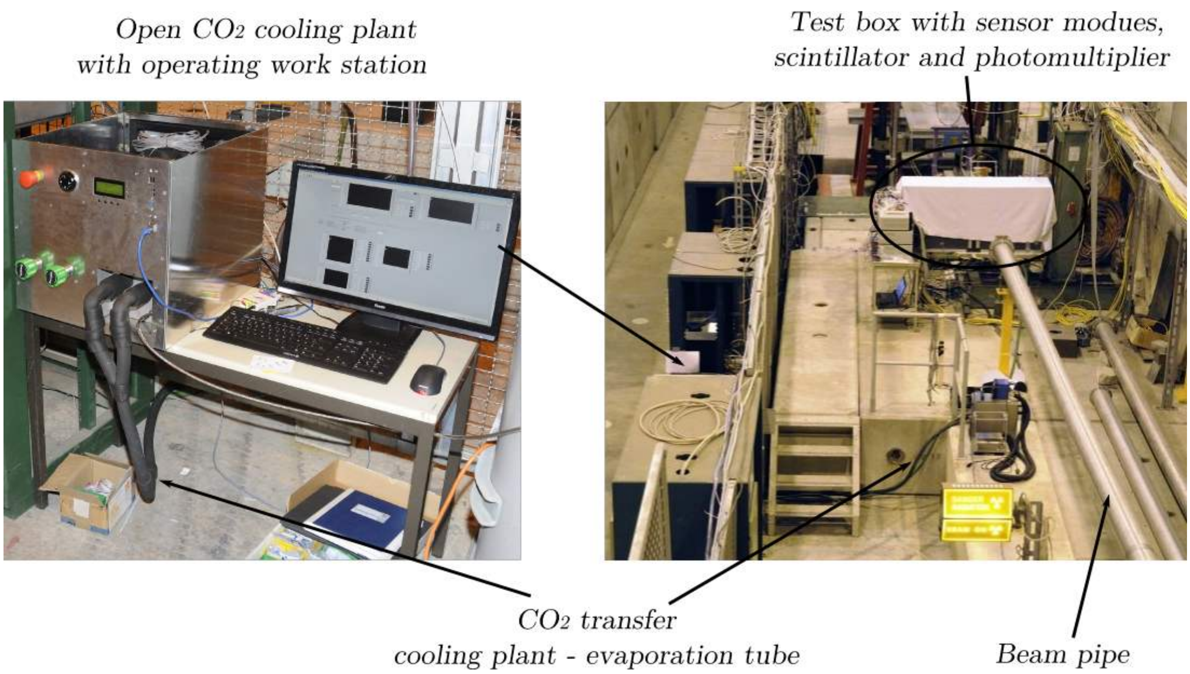

Figure 4.27: Beam test setup at CERN (North Area, SPS secondary beamline H6).

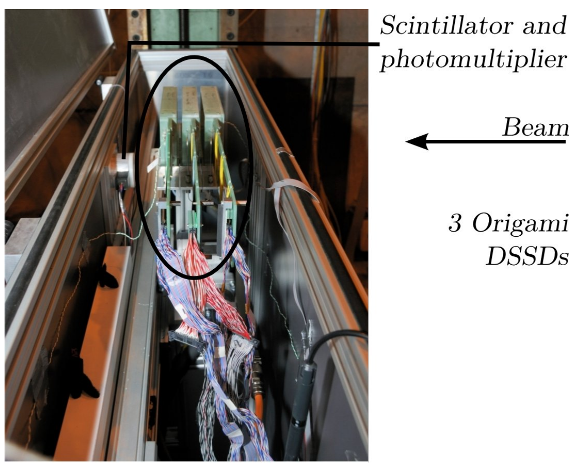

Figure 4.28: Three DSSD modules assembled in the test box.

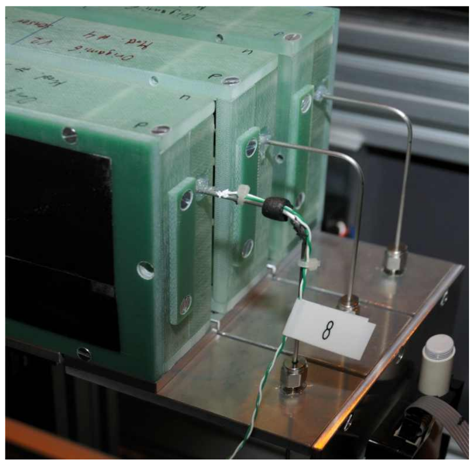

Figure 4.29: Temperature sensor placement at the evaporation tube.

The tube dimensions for this setup were chosen as listed in table 4.2.

Tube	Outer × inner diameter (mm)	Length (m)
Cooling plant to evaporation tube	3.0 × 2.0	8.0
Evaporation tube to cooling plant	4.0 × 3.0	8.0
Evaporation tube/1DSSD	1.6 × 1.0	0.4
Capillary tube	1.6 × 0.5	0.2

Table 4.2: Chosen tube dimensions for the beam test setup.

The open CO_2 cooling system is equipped with many temperature and pressure sensors. Measurement data will be presented in the following section based on selected temperature sensors and one pressure sensor. The two temperature sensors were mounted on the evaporator surface to monitor the tube temperature which can be assumed to be the same as the APV cooling temperature. One sensor is installed before the first Origami module and the second sensor after the third module to observe the APV temperature. The pressure sensor is located inside the cooling plant and measures the evaporation pressure.

4.7.2 Measurements

In this section, some selected measurements from the previously described beam test application will be presented. The given data are $T_{Origami\ in}$, $T_{Origami\ out}$ and the pressure $P_{evaptube}$. The measuring locations are labeled in figure 4.26. The measured values are given without considering any measurement errors. The aim of the measurements is to verify the predicted system behavior and to visualize the coolant's properties as well as the relations between temperature, pressure and mass flow. This test system is optimized to provide constant conditions for the sensor readout electronics to allow reasonable sensor readout with a high signal-to-noise ratio.
The following measurements in figures 4.30 and 4.31 were recorded during a cooling period of about 60 hours. This period is divided into three sections. The first period of about four hours was used for setup and commissioning. During the second period, the cooling system successfully reached a stable pressure and temperature, which were appropriate conditions for sensor module data taking. The last period of about 6 hours was used to investigate the temperature dependence of the APVs. Therefore, the pressure was reduced to achieve a lower evaporation temperature. Figure 4.31 plots the evaporation tube temperatures, the mass flow and the evaporation pressure for period 2 and 3 in more detail.

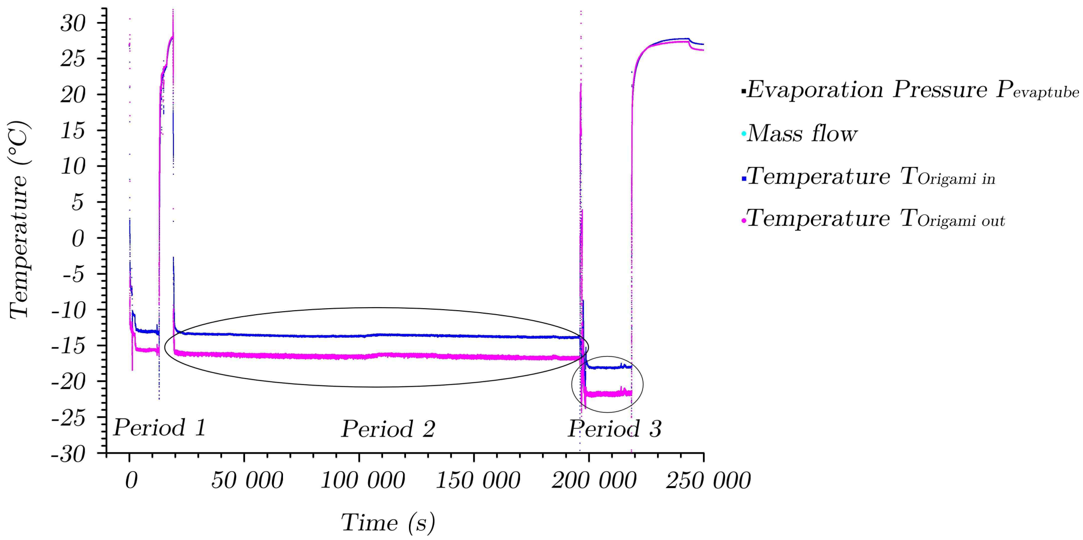

Figure 4.30: Measured evaporation temperatures at the tube surface.

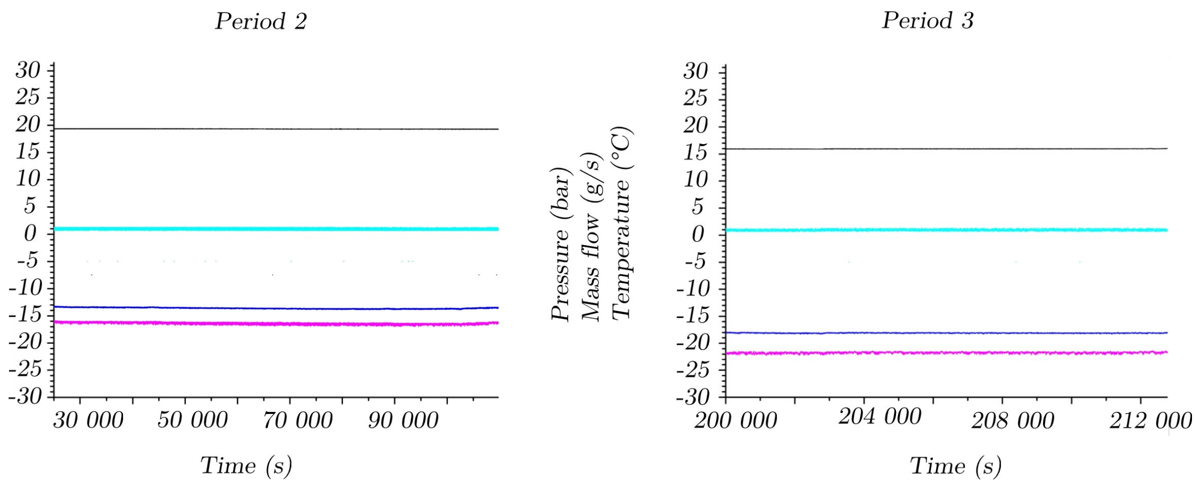

Figure 4.31: Evaporation temperature-, mass flow- and evaporation pressure measurements for two different time ranges period 1 and 2 out of figure 4.30.

For both cooling periods, the mass flow was set to $0.9 gs^{-1}$. The measured temperature difference between the temperature at the beginning and the end of the evaporator can be explained with the pressure drop along the evaporation tube. The pressure drop magnitude consists with the tube dimension. The SVD evaporator diameter is planned to be 0.3mm larger, compared to the evaporator used here. This will result in a lower pressure drop and hence a smaller temperature difference. The resulting temperatures were constant during a few days of operation, indicating a stable cooling system operation.
The measured pressure $P_{evaptube}$ which corresponds to the temperature at the end of the

evaporation tube $T_{Origami\ out}$ was 19bar in the second period and was reduced to 16bar in the third period. The measured values are summarized here:

Cooling period 2			**Cooling period 3**		
$\dot{m}$	=	$0.9gs^{-1}$	$\dot{m}$	=	$0.9gs^{-1}$
$P_{evaptube}$	=	19bar	$P_{evaptube}$	=	16bar
$T_{Origami\ out}$	=	-16°C	$T_{Origami\ out}$	=	-22°C

The CO_2 temperatures at those pressures theoretically are:

T_{evap}(19bar)	=	-21°C	T_{evap} (16bar)	=	-27°C

The measured temperatures varied from the theoretical fluid temperatures because of the measuring method. As shown in figure 4.29, the sensors are installed outside at the tube surface and therefore measure the tube wall temperature. The tube wall resistance as well as the environmental heat load have significant effects on the actual temperature measurement.

4.8 Results

As shown in the previous section, a fully working cooling system was realized and operated. One of the first challenges was to work out the SVD requirements and apply them to the open CO_2 cooling plant. These requirements led to the functional principle, which were represented by a functional block diagram. The component selection was focused on off-the-shelf products, but nevertheless in some cases a prototype component or a special self-developed solution was necessary. A very intensive research phase including discussions with supply firm technicians was necessary to investigate and work out the best solution for the very special requirements of the CO_2 cooling plant. The selection reflects a well-balanced choice of components which fit best the dedicated application and yet keeping in mind the cost efficiency and relevance of the whole plant. Despite all these difficulties, a reliable cooling plant was developed and operated in several applications. Besides the described beam test, it was also operated for the cooling of other applications. Due to the easy adaptability of the realized open CO_2 cooling plant, this system can be used for further development, research and test applications.

Chapter 5

Origami Cooling Design

This chapter is about the design of the readout electronics cooling on the so-called Origami detector modules (Origami cooling design), established by an evaporation tube which is connected to the APVs via a heatsink and mounted at the sensor module by a tube clamping structure. Different heat contact materials and tube attachment structures were tested and evaluated. Section 3.3 lists the requirements which must also be considered for the Origami cooling design. Plastics have been chosen out of several material groups because of being electrically insulating and light-weight. The radiation hardness of a material is a crucial condition for its application inside a particle detector because many plastics are weak to radiation, especially in the SVD with an expected total life time radiation dose of 100kGy.
A major problem concerning the radiation hardness is the insufficient information from manufacturers and distributors. In most cases, details about radiation effects are not or rarely available because those are not required for normal fields of application. CERN provides catalogues on systematic radiation damage test studies. An extract of the study results is given in figure 5.1, where the radiation hardness for different plastic materials is listed. The materials of interest for this chapter are highlighted in blue. These values are very helpful to gain an overview and draw up a shortlist. Nevertheless, dedicated irradiation tests were necessary for the specific application in the Belle II detector.

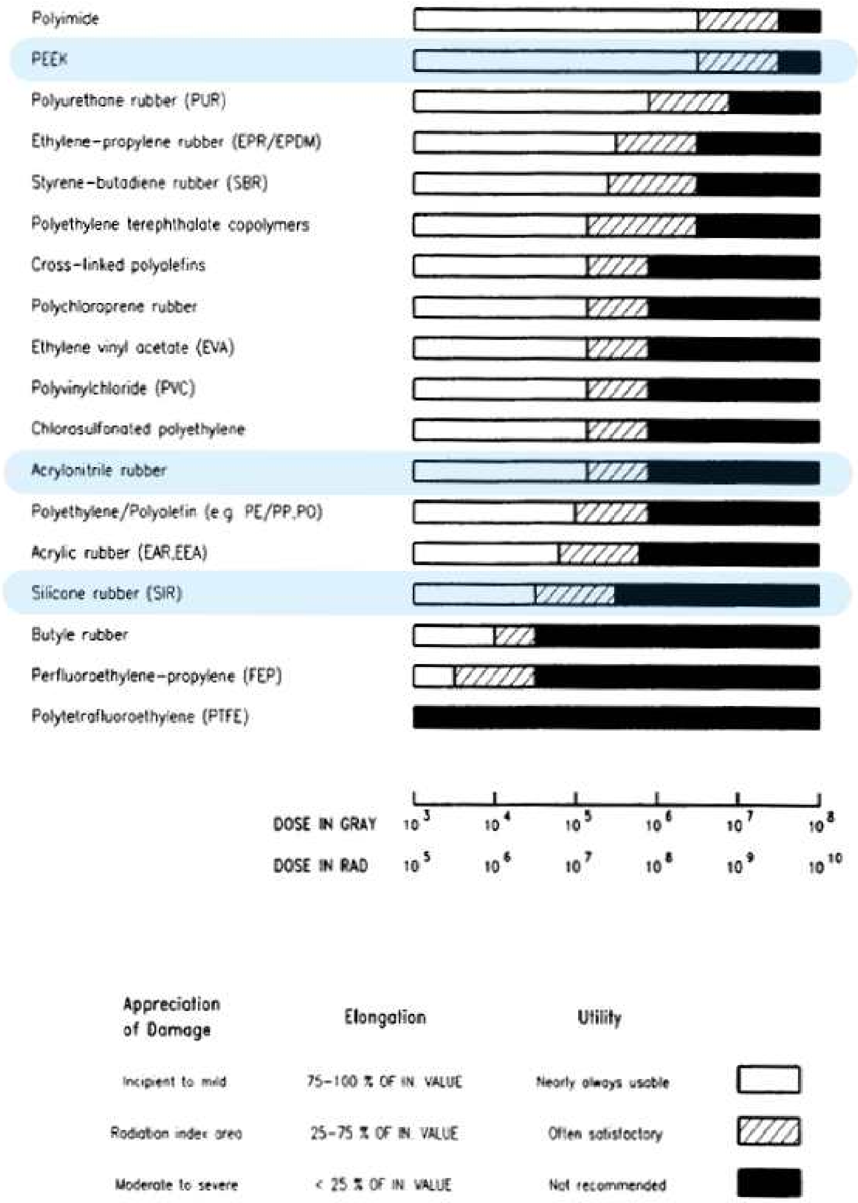

Figure 5.1: Radiation hardness of different materials [43]. Silicone rubber, acrylic rubber and PEEK are of special interest and highlighted in blue.

5.1 Thermal Contact

A thermal contact between the cooling tube and the APVs of the sensor modules must be established for a good cooling. Due to the location of the preamplifier/shaper in the APV25, the cooling tube must be optimally attached edgewise where it is also beneficial for noise reduction. Approximately half of the thermal output of the APV25 is assumed to be absorbed directly under the cooling tube in the preamplifier/shaper region. The following figure 5.2 shows the top view of thermal contact structure and cooling tube alignment.

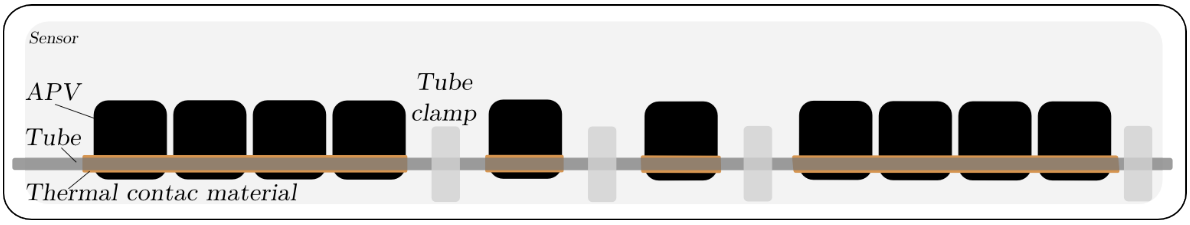

Figure 5.2: An illustration (top view) of the thermal contact structure and cooling tube alignment on top of the APV25 readout chips.

A market analysis was necessary to investigate the availability and applicability of materials which fulfill the requirements for their application in a particle detector. There is a wide market of thermally conductive materials in the electronics sector. Four different types were selected as candidates for the Origami cooling:

- Gap Pads
- Gap filler (two-component, one-component, gel-like, curing, non-curing)
- Heat conductive adhesives
- Heat conductive pastes

All these different material groups include very different application methods which have to be considered together with the material properties. The most promising material which meets almost all requirements is a very soft type of Gap Pad. The specific self-adhesive texture of a Gap Pad enables a relatively clean application. Even in the case of tube dismount, the fragile bond wires will not be destroyed and the APVs will not get detached.
In contrast to Gap Pads, nearly all sorts of Gap fillers tend to cure after application resulting in a severe bond effect which can lead to detached RO chips when tubes are dismounted and removed from the sensor module. The same problem occurs with thermally conductive adhesives, where a firm bonding also causes destruction during disassembly. The application of heat conductive pastes fails mostly because of its consistence. A thermal paste is soft, non-curing and partly suffers from bleeding. All these properties prevent the application for the Origami cooling contact.
Thermally conductive Gap Pads are available in two different types of product categories: rubbers containing silicone and silicone-free rubbers (e.g. acrylic rubbers), where the type containing silicone is more sensitive to radiation.

One important property of plastics like polymers, elastomers and rubbers is their hardness, defined as a material resistance against steady indentation. ASTM D2240 [44] is a standard test method for rubber hardnesses, where the rigidity is given as

durometer hardness. This is also known as Shore hardness, named after the developer of the durometer scale Albert F. Shore. There are twelve different scales of rubber hardness (A, B, C, D, DO, E, M, O, OO, OOO, OOO-S, R), measured with durometers. Each of these scales is divided in values between 0 and 100, with 0 indicating the softest material.
Silicone based polymers have the advantage of a high flexibility over a wide temperature range and a high resistance against vibrations and cracking. Silicone containing rubbers can be very soft, having only a Shore OO hardness of less than 10, compared to chewing gum with a Shore OO hardness of 20. The lower the hardness, the larger the contact area between the tube and the transfer material at an equal amount of acting press-in force. For that reason, soft materials are also able to adjust any unevenness of assembled sensor components, without applying too much force to the module components. Despite all those advantages, materials containing silicone significantly suffer from radiation. Silicone tends to outgassing under irradiation, resulting in modified material texture and the danger of chemical reactions with detector components. Silicone-free rubbers are much harder but less susceptible to radiation. If the contact surface should be in the same order of magnitude than in case of a soft silicone Gap Pad, much more force must be applied to the cooling pipe and therefor to the sensor module.

The radiation dose for the SVD is predicted to be 100kGy within 10 years of operation. For a safe use of materials in the active region of the detectors, the desired materials must undergo radiation tests with a realistic radiation dose. A widespread selection of materials was tested at Mol (Belgium) with a ^{60}Co gamma ray source, according to the required radiation dose of 100kGy. Table 5.1 lists a selection of the numerous tested thermally conductive Gap Pads with their different properties. The decision was made for two very soft Gap Pads containing silicone what is beneficial for a safe assembly, one relatively soft and silicone-free material and one extremely hard silicone-containing and very thin Sil Pad.

	86/125 Keratherm	**2500S20 Bergquist**	**1000SF Bergquist**	**Sil Pad 800 Bergquist**
Hardness (Shore OO)	10	20	40	ShoreA 91
λ ($Wm^{-1}K^{-1}$)	1.5	2.4	0.9	1.6
Thickness (mm)	0.5 – 5.0	0.3 – 6.4	0.3 – 3.2	0.127
Silicone containing	×	×	–	×
Radiation hard (100kGy)	×	–	×	×

Table 5.1: Comparison of different thermal conductive materials with their properties. The material properties are manufacturer's data and the specifications regarding the radiation hardness results from irradiation tests.
[45, 46]

The irradiation test showed insufficient radiation hardness in case of the Gap Pad 2500S20. It is dramatically hardened, it got friable and material residues were noticed when unpacking from the foil where it was covered for the irradiation (figure 5.3).

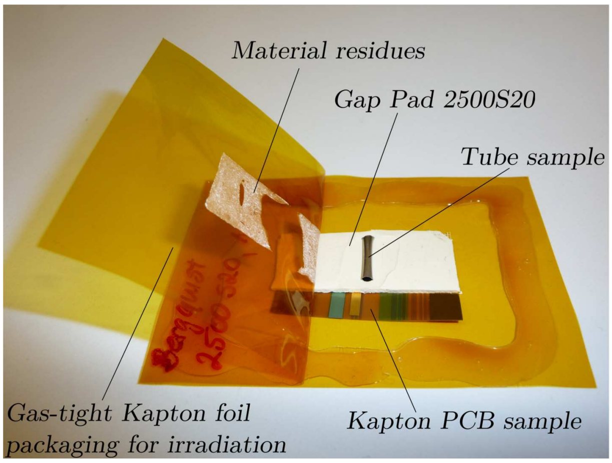

Figure 5.3: A gamma irradiated Gap Pad 2500S20.

Both, the silicone-free Gap Pad 1000SF and the Sil Pad 800 showed adequate radiation hardness at the test irradiation dose. Nevertheless, those materials are not perfectly suitable because of their hardness and in case of the Sil Pad also the texture is adverse. The least affected Gap Pad is the Keratherm 86/125 which is the most promising material for the thermal contact in the Origami module. This Gap Pad is very soft with medium heat conductivity.

5.1.1 Thermal Studies and Prototype Application

The following section discusses thermal studies for two selected heatsink materials: Sil Pad 800 and 86/125 Keratherm. Those were shortlisted for investigations regarding their application in the SVD as described in the previous section. It has to be considered that thermal studies are just simulations with a lot of simplifications which cannot be expected to deliver completely correct results. Nevertheless, the results are meaningful enough for comparing the different materials regarding their properties within constant test setups and study settings. The following listing summarizes the major thermal parameters studied.

- Tube
  - Tube inner surface temperature (coolant temperature): -20°C
  - Material: stainless steel AISI 316L
  - Wall thickness: 0.1mm
  - Tube outer diameter: 1.6mm
- APV

  - Heat load: 0.35W/APV (homogeneously spread over APV; worst case scenario)
  - Material: Silicon
  - Size: 7.10mm × 8.06mm
- Heatsink
  - Size 2mm × 8mm/APV
  - Different Gap Pad materials with varying heat conductivities λ, hardnesses and thicknesses (table 5.2).

	Sil Pad 800	**Gap Pad 86/125**
λ ($Wm^{-1}K^{-1}$)	1.6	1.5
Shore hardness	Shore A 91	Shore OO 10
Thickness (mm)	0.127mm	1.0mm

Table 5.2: Material properties
[45, 46]

Sil Pad 800 Bergquist

Sil Pads inherently differ from common Gap Pads in their thickness and hardness. Sil Pads are much thinner (factor ∼10) and have a much higher Shore hardness. The following thermal study (figure 5.4) shows the thermal performance of the chosen Sil Pad 800.

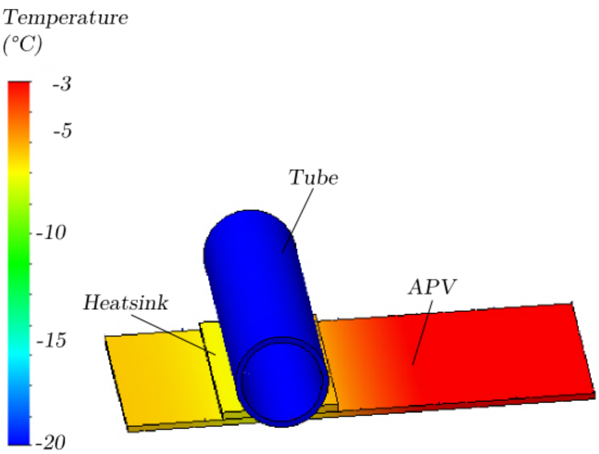

Figure 5.4: Heat transfer simulation of the Sil Pad 800 where the tube is arranged tangential to the heatsink.

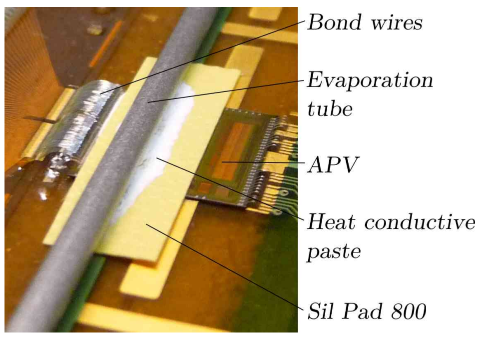

Figure 5.5: A close-up view of the assembled Sil Pad between tube and APV.

The thermal study result for the Sil Pad 800 shows that the heat transfer is rather inefficient. The heat contact surface is quite small due to the very thin and hard heatsink. In this simulation, the heat contact is assumed to be perfect, under real conditions, however this 0.127mm thin Sil Pad is not able to compensate all irregularities.
Figure 5.5 shows an Origami module with an assembled Sil Pad between the APV and the cooling tube. The first Origami cooling test was implemented with the Sil Pad 800. This test setup was without any additional tube fixture (figures 4.25, 5.5), only two bores in the side walls of the box frame determined the tube position. In that case, the tube assembly procedure was very difficult and time consuming because of mechanical inaccuracies of the module and the cooling tube, which is not completely straight. To compensate these irregularities by the Sil Pad 800, large forces would be necessary. An additional heat conductivity paste had to be applied between tube and Sil Pad to ensure a thorough thermal contact.
Despite all those difficulties, a heat contact between all chips and the tube was established and cooling tests could be carried out, using the open CO_2 cooling system.

Gap Pad 86/125 Keratherm

This Gap Pad 86/125 from Keratherm is very soft with a medium heat conductivity similar to the Sil Pad 800. This Gap Pad was simulated (figure 5.6) and tested with two different layer thicknesses, 0.5mm and 1.0mm. In both cases, the distance between tube and APV is 0.4mm, implying a tube penetration depth of 0.1mm in case of the thin pad and 0.6mm in case of the thick pad.

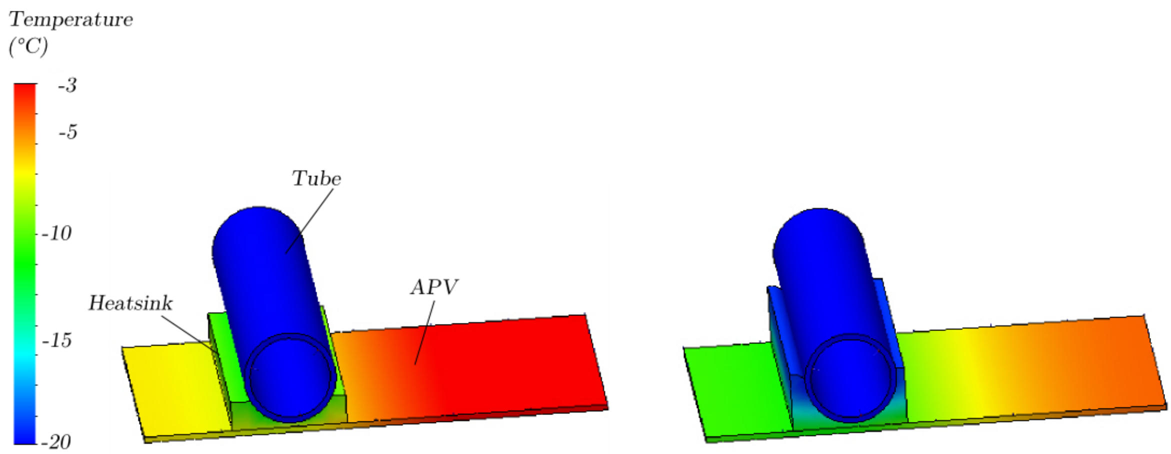

Figure 5.6: Simulations of the heat transfer between cooling tube and APV with 0.5mm and 1.0mm thick Keratherm 86/125 Gap Pads. In both cases the distance between APV and tube is 0.4mm.

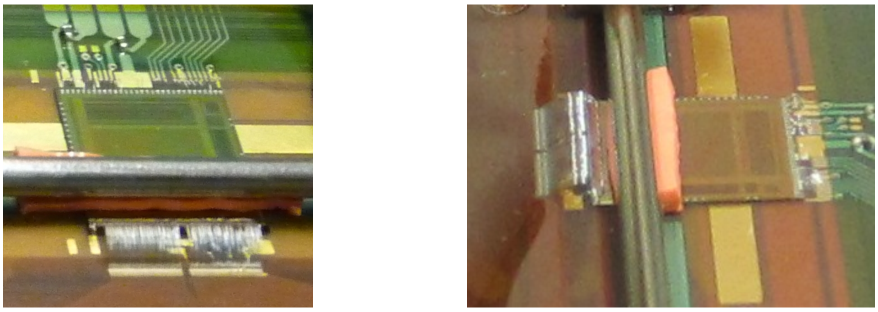

Figure 5.7: A close-up view of the Origami module, showing the 0.5mm and 1.0mm thick Gap Pad 86/125, respectively, assembled between APV and tube.

The study result (figure 5.6) for the thin Keratherm is akin to the very thin but slightly higher thermally conductive Sil Pad 800. The study shows that the heat transfer can be significantly improved with a thicker Gap Pad because of the increased contact surface between tube and heatsink.
This very soft Gap Pad also meets all requirements concerning the assembly procedure including the claimed large contact area between tube and Gap Pad. For assembly and cooling tests of the RO chips, an Origami module was equipped with the Gap Pad 86/125 (figures 5.7, 5.14). The actual preparation was easy because of the Gap Pads softness and its little sticky texture, thus avoiding shifting of the Gap Pad at the module. The low degree of hardness results from its relatively high silicone content, but as proven in the irradiation test, the material texture is only very slightly affected by radiation and hence usable for the particle detector application. The applied radiation dose only caused minimal hardening of the material but it kept its sticky and soft texture and could be dismounted without leaving any residues.

5.1.2 Application Results

For cooling tests of the readout chips, several Origami modules were equipped with cooling tubes and thermally conductive materials. As mentioned earlier, the assembly process is very critical and an adequate heat contact is difficult to realize due to some tolerances of the surface planes and heights of the individual APV25 chips and the very fragile sensor module structure.
To prevent damages of the sensor modules, a minimal acting force at the assembly procedure is mandatory. Nevertheless, the thermal contact must be sufficient which could be best achieved with the Keratherm Gap Pad, especially with the 1.0mm thick version. A compromise between thermal properties and handling must be found. Due to the investigations reported above, the Keratherm Gap Pad meets the requirements for an application at the SVD better than the other tested materials.
This first tube assembly procedures and Origami cooling tests have shown the necessity of a suitable tube mounting structure to make the tube mounting safe and straightforward and also to improve the thermal contact.

5.2 Tube Attachment

The SVD cooling tubes must be attached on top of the Origami sensor modules. It is planned to cool several ladders with one cooling coil. This requires several tube fixing points at the ladders to ensure an efficient thermal contact and to avoid damages of the very fragile sensor modules. Therefore, the SVD cooling necessarily needs a kind of tube holder clamp. This section deals with the design and evaluation of different clamp types.

5.2.1 Requirements

The Origami modules of the SVD are very complex detector components. The tube clamps must be directly assembled on top of the sensor modules, inside the active detector region. For that reason all requirements regarding an additional material in the detector volume from section 3.3 also apply here. The most important aspects are listed in the following and must already be taken into account during the design process.

- Ensure an adequate heat contact between APVs and evaporation tube.
- Designed in a small geometry (material budget).
- Mountable in a safe way.
- Feature a guideway for the cooling tube at the tube assembly procedure.
- Safely attach the cooling tubes during operation under pressure and at evaporation temperature.
- Enable removing/ remounting of the evaporation tube.
- Mounted without performing mechanical stress to sensor.
- Avoid mechanical stress resulting from thermal expansions.
- Manufactured from a machinable and radiation hard material.

5.2.2 Material Selection

A machinable material must be found which meets all the requirements for its application in a particle detector. Due to its superior radiation resistance as shown in figure 5.1, PEEK (Polyether ether ketone) was chosen and its machinability tested in several prototypes. PEEK is a high performance organic polymer thermoplastic with an excellent thermal stability. Thanks to its exceptional resistance to high gamma radiation dose, it is a perfect candidate for applications in a particle detector.

5.2.3 Design, Simulation and Prototypes

A prototype production means a production of only few parts, with realistic dimensions and materials to get functioning samples. Finding a well performing prototype needs different designs and samples, for which an applicable and cost efficient production method must be found. To produce realistically working prototypes for test arrangements, the precision of the prototypes must be just as high as for the final model. Table 5.3 compares the most relevant characteristics of a selection of different production methods. For an easy and inexpensive production, 2D production techniques are preferred.

	Milling	**Micro water jet cutting**	**Rapid prototyping**	**Laser cutting**
Fabrication tolerance (mm)	$\pm$ 0.1 in HEPHY's workshop	$\pm$0.01	$\pm$0.1mm	$\pm$0.1 for plastics
Material machinability	nearly all	nearly all	highly restricted	restricted
Price	low	medium	medium	medium

Table 5.3: A comparison of different production methods and their most relevant properties. The values are based on manufacturer's data.

For functional tests, it is essential to produce the prototypes in their final materials at affordable costs. Rapid prototyping methods can be dropped, because the radiation hardness of the usable materials is not sufficient. Methods, with which the chosen materials could not be machined in the required precision, e.g. laser cutting methods, are also not an option. Finally, the best choice turns out to be water jet cutting, which can be applied to most plastics, including PEEK.
Micro water jet cutting fulfills all requirements and therefore is an adequate prototyping method for the tube clamps. Table 5.4 compares the micro water jet cutting with the conventional water jet cutting. The most meaningful difference is the higher precision by one order of magnitude of micro water jet cutting, allowing smaller geometries to be produced. The manageable minimal inner diameter by micro water jet cutting allows much smaller structures which are needed for the tube clamps.

	Water jet cutting	**Micro Water jet cutting**
Fabrication tolerance (mm)	±0.1	±0.01
Max. thickness (mm)	50	20
Positioning accuracy (mm)	±0.03	±0.003
Min. inner radius (mm)	0.4	0.1

Table 5.4: A comparison of the conventional water jet cutting and the much more precise micro water jet cutting.

For first function tests, a number of different clamp prototypes were designed and manufactured by different production methods. In the following section, the different design types are listed and evaluated regarding their applicability at a particle detector. Based on the sensor module structure, the installation method of all clamp types is the same, they can be installed only by gluing on top of the Kapton PCB.

One part spring-clamp-v1

The one part spring-clamp-v1 is a simple design, which was produced in the HEPHY's workshop by milling. Subsequently, the 3D model from the one part spring-clamp-v1 and prototypes are depicted in figures 5.8 and 5.9.

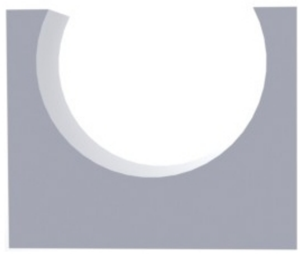

Figure 5.8: A 3D model of the one part spring-clamp-v1. The thickness of the clamp is 1.0mm and the tube notch has a diameter of 1.6mm.

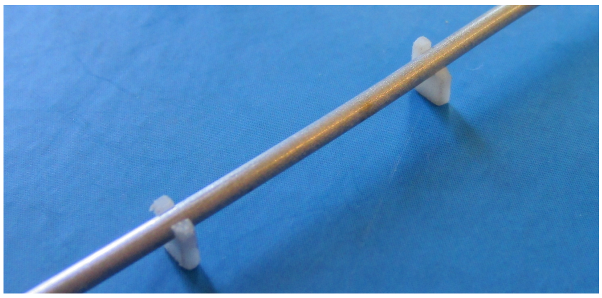

Figure 5.9: One part spring-clamp-v1 prototypes, assembled with an evaporation tube.

This rather simple design was applied to 1.0mm thick glass fiber reinforced plastic. Besides its advantageous simple design, the prototype revealed some problems. A relatively great force is needed in order to snap the tube into the clamp. In addition, the side wall structure is not adequate. The needed flexibility to clamp the tube implies fragility and the clamp wings tend to break easily. The preproduction model (figure

5.9) is difficult to handle during manufacturing and also at the installation process due to its very tiny geometry. Also the smallish contact surface aggravates the positioning and gluing process.

Two part screw-clamp

The next design is a two part draft of 4mm thick glass fiber reinforced plastic. The two parts are screwed together by two small M2 screws to jam the tube between the two parts of the clamp (figure 5.10).

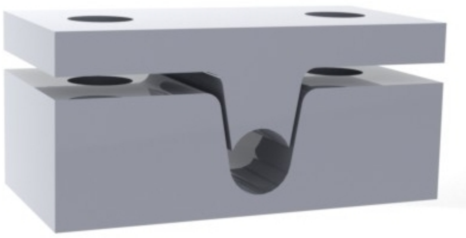

Figure 5.10: A 3D model of the two part screw-clamp. The thickness of both parts is 4mm. The notch for the evaporation tube has a diameter of 1.6mm.

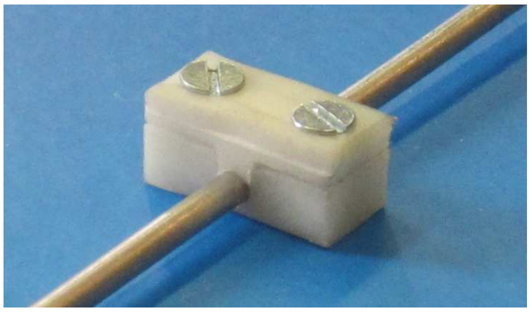

Figure 5.11: A prototype of the two part screw-clamp assembled with a cooling tube.

Figure 5.11 shows the two part screw-clamp prototype together with the cooling tube. The driving reason for the resulting relatively big size is the screw mechanism and the necessary material for chuck jaw clamping at drilling. This design has some disadvantages:

- It is too bulky for the application with the Origami modules in the SVD.
- It does not meet the material budget requirements.
- There is a danger of damaging the sensitive sensor modules, especially the bond wires, with the screws, the loose clamp top part and the screwdriver during assembly.

Two part hinge-clamp

The mentioned disadvantages of the shown two part screw-clamp led to the design of the two part hinge-clamp which follows another design concept. The screw locking mechanism is replaced by a clamping mechanism. With the hinge-clamp design, the amount of material could be significantly reduced and screws and additional tools for the installation are no longer required. Figure 5.12 shows a 3D model of the designed hinge-clamp.

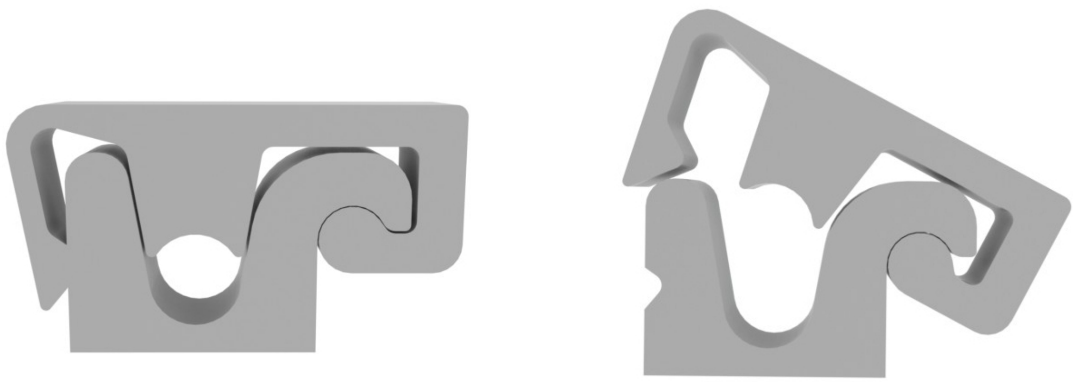

Figure 5.12: A 3D model of the hinge-clamp. The thickness of the top and bottom clamp parts is 2.5mm. The diameter of the tube notch is 1.6mm.

The design shown in figure 5.12 was verified by a simulation and optimized considering the necessary acting force for its snap-in mechanism. The main design requirement was to keep the acting force as low as possible to avoid damage to the sensor. Based on experience, the acting force for the snap in mechanism should be about 1.4N. With the help of a CAD simulation tool, the design was adjusted to this value. By evaluating simulation results, it has to be considered that simulation studies do not provide exact values but nevertheless, they are necessary and helpful for the design process.
Prototypes were manufactured out of PEEK and machined by micro water jet cutting. This design has qualified for installation at a 2DSSD[1] sensor module prototype. The module was equipped with three hinge-clamps per sensor where they were directly glued onto the Kapton PCB with a thin film of epoxy resin. Therefore, the clamp bodies were crudely placed with a tweezer and afterwards exactly adjusted in a row with the tube. After adjusting the clamp bodies in their exact position and the curing of the glue, the clamp caps were mounted in the foreseen hinge of the clamp bodies and snapped in. Figure 5.13 depicts the hinge-clamp assembly procedure on a sensor module.

[1] 2DSSD stands for a detector prototype module comprising of two double-sided silicon strip detectors arranged next to each other.

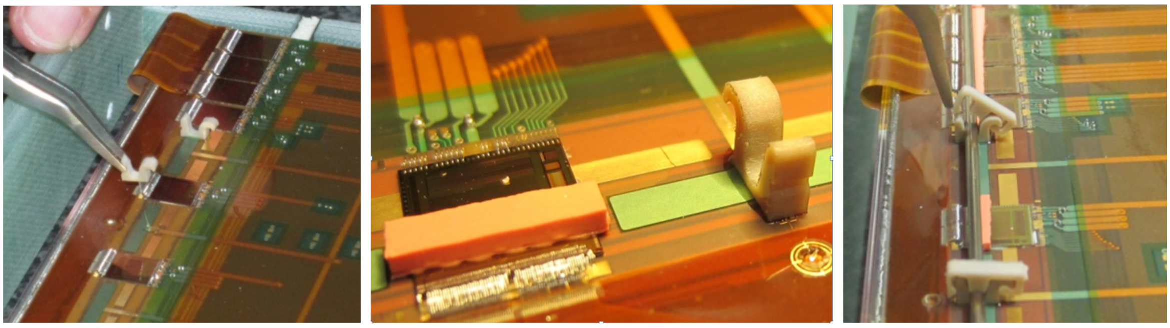

Figure 5.13: The assembly procedure of the hinge-clamp on an Origami sensor module.

The first prototype test of this clamp design showed that the clamping force is far lower than desired. It turned out that the predicted 1.4N from the simulation were actually 0.3N for the real prototypes. The distance between tube surface and APV is designed to be 0.4mm. The resulting clamping force which was provided by the first prototype clamp was not enough to push the tube 0.6mm into the very soft 1.0mm thick Gap Pad 86/125. Therefore, the thinner (0.5mm) Gap Pad was used. Test results showed that a sufficient thermal connection between the tube and each APV was reached but with a very small contact surface. The completely assembled evaporation tube on the 2DSSD Origami module is pictured in figure 5.14.

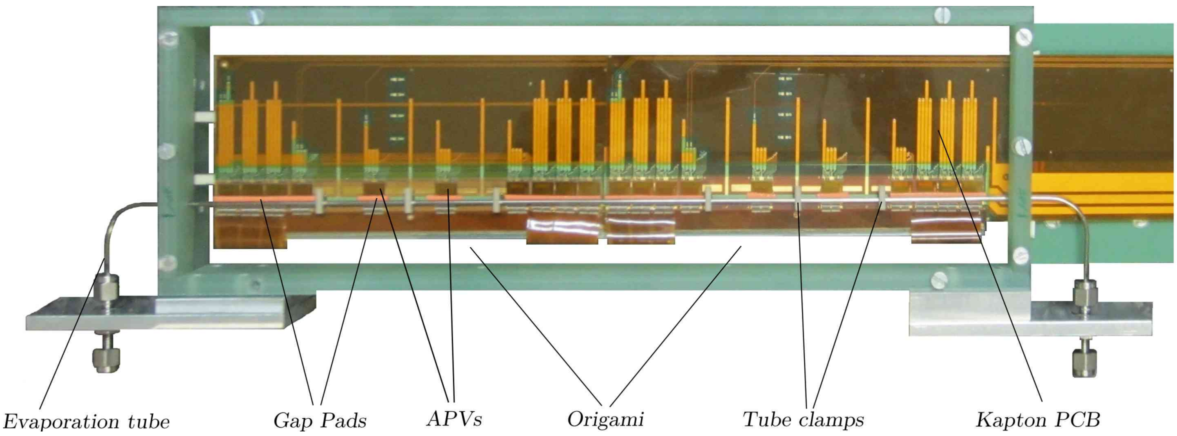

Figure 5.14: A 2DSSD Origami module prototype with an assembled cooling tube, hinge-clamps and 86/125 Keratherm Gap Pads.

One part spring-clamp-v2

A further design, the one part spring-clamp-v2, was developed to simplify the production and assembly procedure even more. It was also manufactured by micro water jet cutting from PEEK, whereby the design could profit from the experience from the former hinge-clamp design. The corresponding 3D model of the spring-clamp-v2 design is shown in figure 5.15. The underlying working principle of this clamp is similar to one part spring-clamp-v1, but with an improved, much more robust design. For the spring-clamp-v2, the resilient parts are longer and thicker. Compared to the previous two part designs, the spring-clamp-v2 promises a much easier handling. It is designed with a higher press-in force, about one and a half time stronger than the press-in force of the hinge-clamp design. This concept was realized in two different versions with a varying spring force to verify the simulation results and the applicability.

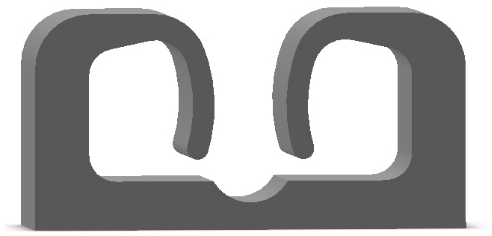

Figure 5.15: A 3D model of the spring-clamp-v2 with a thickness of 2.5mm and a tube notch diameter of 1.6mm.

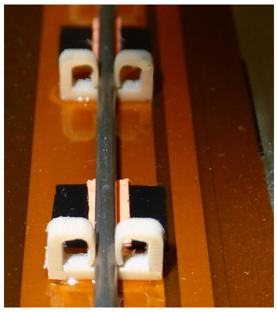

Figure 5.16: Assembled spring-clamp-v2 prototypes with an evaporation tube.

To test the functionality of the spring-clamp-v2 regarding its applicability in the SVD, a layer 6 mockup was assembled. Similar to the hinge-clamp, the real clamping force at the prototypes is much lower than the study stated. Measured values with a spring balance range between 0.6N and 0.8N for the version where the study predicted 2.4N and between 0.9N and 1.4N for the version, where the study predicted 5.4N.
This design revealed an excellent manageability in the mockup application. The clamps are simple to handle during the gluing process and after curing and they perfectly guide the tube during the tube application. Thus the risk of damaging the module through loose parts is mitigated. Moreover no tools are required for the tube remount; it can be pulled out just by grasping the tube on the forward or backward side at a safe distance from the sensor. Another positive fact is the cost efficient and simple production by 2D water jet cutting. Based on these positive aspects, both the slightly weaker and also the little stronger clamp versions suits for the cooling tube attachment. In case of the SVD cooling application the decision was made for the little tighter clamp version.

5.2.4 Clamp Design Results

The assembly tests with the different clamp prototypes have proven that clamping mechanisms generally are suitable for the Origami and are required for tube mounting onto the SVD ladders. Compared to the very first tube assembly procedure without any tube attachment to the sensor module (figure 4.25), the establishment of an effective thermal contact with a tube fastening clamp is much easier and safer (figure 5.14). It functions as a guideline for the tube at the installation process and thus reduces the risk of damaging the sensor or the bond wires. The spring-clamp-v2 design turned out to be the best choice because of its rather simple design and excellent handling.

At this development process, micro water jet cutting was found to be best method to machine prototypes out of PEEK. The chosen machining method together with the evaluated material results in an excellent working prototype. This manufacturing method is also well applicative for series production because the required quantity does not exceed 1000 pieces.

5.3 Cooling Material Budget of an Origami Module

Subsequently, the material budget of all Origami cooling components is calculated, using equation 3.8. An Origami module consists of one DSSD with all the necessary mechanical, electronic and cooling components. Although the material budget of an Origami module is dominated by the silicon sensor, the cooling material budget also contributes. The evaporation tube represents the major part and, besides that, one must also consider tube fixing clamps, heat contact material and the refrigerant.
The respective average radiation lengths are calculated for different tube dimensions, refrigerants, heat contact materials and tube mounting structures, without considering the negligible glue film. The corresponding results are summarized in table 5.5, where the respective radiation lengths are given in mm.

Tubes and refrigerants

The former Belle SVD used water as refrigerant, flowing in aluminum pipes. There, no active cooling was necessary due to the former detector design. The new SVD design together with the Origami chip-on-sensor design requires an active cooling installed inside the active detector volume. Much more tube and coolant material would be necessary when using H_2O as coolant flowing in aluminum tubes compared to the new CO_2 cooling concept with CO_2 and significantly thinner stainless steel tubes.
The radiation length of aluminum with X_0=89.0mm is approximately 5 times higher than that of stainless steel with X_0=17.2mm, but nevertheless the overall radiation length could be increased using the new design. The shorter radiation length of stainless steel can be compensated by the coolant's radiation length, where CO_2 (X_0=905.0 – 4827.0mm, depending on its phase) outperforms water (X_0=360.5mm) and will be also used in smaller quantity.

Heat contact material

An average radiation length of X_0=200.0mm is assumed for the heatsink material which establishes an acceptable heat contact between the APVs and the cooling tubes, based on experience values. This assumption must be made because of poor manufacturer information. An approximate calculation could also not be made because of missing details about the materials chemical compositions. The only effect which can be considered is the impact resulting from the differing thicknesses.

Table 5.5 compares three different material thicknesses, where the heatsink material is assumed to be 8mm × 2mm per APV. Ten APVs must be thermally contacted to the evaporation tube on every module. The results for the average material budgets of the different heat contact material geometries contributing to the overall module material budget are listed in table 5.5.

Tube mounting structure

The material selection of the tube mounting structure is restricted by a lot of requirements (section 5.2.1). PEEK (Victrex PEEK G450) is planned to be used for the tube fixing clamps of the SVD. As in the case of the heat contact material, material properties regarding the radiation length of PEEK are missing, too. Based on experience and literature survey, the radiation length of PEEK is assumed to be X_0=315.0mm. For the following calculation, the 'spring-clamp-v2' volume of about 40mm^3 is used. The average material budget of the tube mounting structure is listed below in table 5.5.

Average material budget

The radiation length values used in the following table are mostly given by the Particle Data Group [47] and are partly assumptions, as described above. The dimensions of the tubes are given with outer × inner diameter and the refrigerant dimensions equal the inner evaporation tube diameters. In case of the heatsink the dimensions refer to the size of one pad, while ten pieces are necessary for one Origami module. Similarly, the given dimension of the tube clamp refers the volume of one clamp, while three clamps are needed for each module. Equation 3.8 is used for calculating the average material budget, where the sensor area A_0 is 7438.1mm^2 (sensor dimensions: 59.6mm × 124.8mm).

	Material	Dimensions (mm)	$\mathbf{X}_0$ (mm)	$\frac{t_i A_i}{A_0}$ (mm)	$\frac{X}{X_0}$ (%)
Tube	Aluminum	2.0 × 1.6	89.0	0.019	0.021
	Stainless steel AISI 316L	1.6 × 1.4	17.2	0.008	0.046
		1.6 × 1.5	17.2	0.004	0.024
Refrigerant	H_2O	1.6	360.5	0.034	0.009
	CO_2 liquid (gaseous 8%)	1.4	905.0	0.026	0.003
		1.5	905.0	0.030	0.003
	CO_2 gaseous (gaseous 75%)	1.4	4827.0	0.026	0.001
		1.5	4827.0	0.030	0.001
Heat contact (10/Origami)		8 × 2 × 0.127	200.0	0.003	0.001
		8 × 2 × 0.5	200.0	0.011	0.005
		8 × 2 × 1	200.0	0.022	0.011
Tube clamp (3/Origami)	PEEK G450 (Victrex)	40mm^3	315.0	0.016	0.005

Table 5.5: The average material budget $\frac{X_i}{X_0}$ for different materials and dimensions.

The overall average Origami cooling material budget is the sum of all values of the several assembly components. According to the current design, the SVD Origami cooling will be implemented with the following components:

- Stainless steel tube 1.6mm outer diameter, 0.1mm wall thicknesses
- CO_2 as coolant
- Keratherm 86/125 1.0mm thicknesses for thermal contact (ten per module)
- PEEK tube fixing clamp 'spring-clamp-v2' (three per module)

The resulting average Origami cooling material budget for this setup is 0.063%. This calculation is based on the Belle II design report [5] and is adjusted for the CO_2 cooling concept with tube fixing clamps. The CO_2 cooling with all its necessary components accounts only for slightly more than one tenth of the total material budget of each module, which is dominated by the silicon sensor, which contributes with 0.320% [5].

5.4 Results

The investigations and the development process in this chapter evolved towards a well designed cooling. The chosen Gap Pad, together with the designed tube fixing clamp ensures a highly efficient thermal contact and, at the same time, it is a comfortable and risk minimizing support at the module assembling procedure. The development of this Origami cooling design was only possible in combination with the open CO_2 plant to simulate the SVD cooling under similar conditions.

Chapter 6

Conclusion

In the course of this thesis, a satisfying cooling design could be worked out and a properly working, stable and flexible cooling system was constructed and finally applied in several cooling applications. It has been shown that an open CO_2 cooling system is appropriate to become familiar with CO_2 as coolant and to perform cooling tests with real sensor module prototypes.

This thesis describes the working principle in detail as well as the used components, the properties of the cooling plant and its application. First of all, a description and analysis of the Belle II SVD cooling is given and the resulting requirements are worked out. Considering these special requirements, an open CO_2 cooling system concept was developed. This concept was converted through a challenging and extensive CAD design phase in a realistic and detailed construction plan. The component selection and dimensioning was a part of the design phase. More extensive investigations were necessary to meet all demands concerning the functionality. Several iterations and a good physics understanding were required to work out such a widely adjustable and powerful cooling plant. The component selection was a time consuming process but justified due to the usage of off-the-shelf components whereby development resources could be saved. Through the careful preparation, the assembly procedure and commissioning of the cooling plant went ahead without problems. The unproblematic commissioning instantly allowed first test runs with a simple experimental setup using dummy heat loads. First operations brought insights in CO_2 properties and the plant behavior.
Another major issue is the development of the Origami cooling design for which investigations were made. There, the focus was set on the thermal contact between RO chips and cooling tube and on an appropriate tube attachment structure. After establishing the elaborated concept, a well performing prototype was successfully tested with the open CO_2 cooling system.

The developed cooling plant performed excellently at several beam tests where sensor module prototypes were operated with the evaporative CO_2 cooling as it will be finally used for the SVD. Due to the sophisticated design and construction, the plant successfully operated at long term runs for several days. This developed plant contributed in gaining experience with two phase evaporative CO_2 cooling and showed its excellent function in practice. It enabled the development and testing of a proper Origami cooling concept and is ready to be used for detector ladder cooling for series production.

Bibliography

[1] S. Kikutani and E. Kurokawa. Overview of the KEKB accelerators. *Nucl.Instrum.Meth.*, A499:1–7, 2003.

[2] M. Kobayashi and T. Maskawa. CP-Violation in the Renormalizable Theory of Weak Interaction. *Progress of Theoretical Physics*, 49(2):652–657, 1973.

[3] A. Abashian, K. Gotow, N. Morgan, L. Piilonen, S. Schrenk, et al. The Belle Detector. *Nucl.Instrum.Meth.*, A479:117–232, 2002.

[4] Z. Dolezal. Super KEKB and Belle II: status of the KEK SuperB factory. *PoS*, HQL2010:079, 2010.

[5] T. Abe et al. Belle II Technical Design Report. *KEK (High Energy Accelerator Research Organization) Institute of Particle and Nuclear Studies*, 2010.

[6] M. Zobov, C. Milardi, P. Raimondi, E. Levichev, P. Piminov, et al. Beam dynamics in crab waist collisions at DAFNE. *ICFA Beam Dyn.Newslett.*, 48:23–33, 2009.

[7] S. (ed.) Hashimoto, M. (ed.) Hazumi, J. (ed.) Haba, J.W. (ed.) Flanagan, Y. (ed.) Ohnishi, et al. Letter of intent for KEK Super B Factory, Part III: Accelerator Design. Technical report, KEK. 2004.

[8] Belle II. http://belle2.kek.jp/.

[9] C. Marinas. The Belle-II pixel vertex tracker at the SuperKEKB flavour factory. *Nucl.Instrum.Meth.*, A628:95–98, 2011.

[10] A. Owens and A. Peacock. Compound semiconductor radiation detectors. *Nucl.Instrum.Meth.*, A531:18–37, 2004.

[11] M. Krammer. Lecture notes Teilchendetektoren, 2009.

[12] Y. Iwata, T. Ohsugi, K. Fujita, H. Kitabayashi, K. Yamamoto, et al. Optimal P-stop pattern for the N-side strip isolation of silicon microstrip detectors. *IEEE Trans.Nucl.Sci.*, 45:303–309, 1998.

[13] I. Gfall. Mechanical Design of the Belle II Silicon Vertex Detector. Diploma thesis at the University of Vienna. 2013.

[14] M.J. French et al. Design and results from the APV25, a deep sub-micron CMOS front-end chip for the CMS tracker. *Nucl.Instrum.Meth.*, A466:359–365, 2001.

[15] C. Amsler et al. Review of Particle Physics (RPP). *Phys.Lett.*, B667:1–1340, 2008.

[16] W.M. Yao et al. Review of Particle Physics (RPP). *J.Phys.*, G33:1–1232, 2006.

[17] Y. Tsai. Pair Production and Bremsstrahlung of Charged Leptons. *Rev.Mod.Phys.*, 46:815, 1974.

[18] M. Van Beuzekom, A. Van Lysebetten, and B. Verlaat. CO2 cooling for HEP experiments. *TWEPP paper*, 2008.

[19] B. Verlaat. Controlling a 2-phase CO2 loop using a 2-phase accumulator. *International Congress of Refrigerantion, Beijing*, ICR07-B2-1565, 2007.

[20] A. A. M. Delil, M. Dubois, and W. Supper. In-orbit demonstration of two-phase heat transport technology - Status of TPX II: The European two-phase experiment reflight. *Sixth European Symposium on Space Environmental Control Systems, held in Noordwijk, The Netherlands*, SP-400:p. 355, 1997.

[21] Olaf Behrendt. The LHCb vertex locator. *Nucl.Instrum.Meth.*, A598:61–63, 2009.

[22] Sadakazu Haino. The AMS-02 silicon tracker. *ICATPP Conference*, pages 173–180, 2010.

[23] B. Verlaat, A. Woering, A. Pauw, and A. A. M. Delil. AMS-2 Tracker Thermal Control System: design and thermal modeling of the mechanically pumped two-phase CO2 loop. *AIAA Aerospace Sciences Meeting & Exhibit*, 2003.

[24] United Nations Environment Programme. *Handbook for the Montreal Protocol on Substances that Deplete the Ozone Layer*. Ninth edition. Secretariat for The Vienna Convention for the Protection of the Ozone Layer & The Montreal Protocol on Substances that Deplete the Ozone Layer , 2012.

[25] United Nations. Framework Convention on Climate Change.

[26] United Nations. Conference on Environment and Development. 1992.

[27] United Nations. Kyoto Protocol to the United Nations Nationals Framework Convention on Climate Change. 1998.

[28] S. Kandlikar et al. *Heat transfer and fluid flow in minichannels and microchannels.* Elsevier, 2005.

[29] J. Pettersen et al. Heat transfer and pressure drop for flow of supercritical and subcritical CO2 in microchannel tubes (TR A5127). 2000.

[30] J. R. Thome and J. G. Collier. *Convective Boiling and Condensation.* Oxford University Press Inc., New York, third edition, 1994.

[31] G.Ding and C. Zhang. Approximate analytic solutions of adiabatic capillary tube. *International Journal of Refrigeration*, 27:17–24, 2004.

[32] Swagelok. http://www.swagelok.com/.

[33] SAMSON. *Arbeitsblatt zur Ventilberechnung, KV-Wert - Ventilauslegung*, 2012.

[34] PARCOL. *Handbook for control valve sizing.*

[35] ARKEMA Innovative Chemistry. http://www.arkema.com/.

[36] T. Wetzel and P. Böckh. *Wärmeübertragung: Grundlagen und Praxis.* Springer, 2009.

[37] SWEP. http://www.swep.net/.

[38] Armacell. http://www.armacell.com/.

[39] GE Measurement & Control. http://www.ge-mcs.com/en/flow/coriolis.html.

[40] Maxim Integrated. http://www.maximintegrated.com/.

[41] Danfoss. http://www.danfoss.com/.

[42] ALIX system boards. http://www.pcengines.ch/alix.htm.

[43] M. Tavlet, A. Fontaine, and H. Schonbacher. Compilation of radiation damage test data. 1998.

[44] ASTM D2240 Standard Test Method for Rubber Property. http://www.astm.org/Standards/D2240.htm.

[45] Kerafol. http://www.kerafol.de/.

[46] Bergquist. http://www.bergquistcompany.com/.

[47] Particle Data Group. http://pdg.lbl.gov/2011/AtomicNuclearProperties/.

Danksagung

Ich bedanke mich bei Herrn Prof. Dr. Fabjan und Herrn Dr. Friedl vom Institut für Hochenergiephysik der Österreichischen Akademie der Wissenschaften für die Betreuung meiner Diplomarbeit. Vielen Dank für die Möglichkeit der Mitarbeit an diesem internationalen Forschungsprojekt. Für eine gute und produktive Zusammenarbeit danke ich allen Kollegen am Institut, besonders Immanuel und Thomas für die schöne gemeinsame Zeit im Büro.

Meinen Eltern und meiner Schwester danke ich herzlich für ihre Unterstützung. Sie haben meinen Bildungsweg geprägt und sind mir auf diesem Weg mit viel Unterstützung und Rückhalt zur Seite gestanden. Mein aufrichtiger Dank geht an meinen Freund Luka für die vielen ermutigenden Worte, die liebevolle Unterstützung, die vielen fachlichen Diskussionen und die mir gegenüber aufgebrachte Geduld. Mein Dank geht auch an Vjera für ihre wertvollen und aufwertenden Korrekturen.

Lebenslauf

Persönliche Daten

Annekathrin Frankenberger

Schulausbildung

09/2005 – 07/2006	Fachoberschule (Fachgebundene Hochschulreife)

Studienverlauf

10/2006 – 04/2013	Diplomstudium Physik Titel der Diplomarbeit: Development of an Open CO_2 Cooling System for Belle II

Wien, April 2013